PLOS ONE

RESEARCH ARTICLE

A model for studying the energetics of sustained high frequency firing

Bela Joos[1,2]*, Michael R. Markham[3], John E. Lewis[2,4], Catherine E. Morris[2,5]

1 Department of Physics, University of Ottawa, Ottawa, Ontario, Canada, **2** Center for Neural Dynamics, University of Ottawa, Ottawa, Ontario, Canada, **3** Department of Biology, The University of Oklahoma, Norman, Oklahoma, United States of America, **4** Department of Biology, University of Ottawa, Ottawa, Ontario, Canada, **5** Neuroscience, Ottawa Hospital Research Institute, Ottawa, Ontario, Canada

* bjoos@uottawa.ca

OPEN ACCESS

Citation: Joos B, Markham MR, Lewis JE, Morris CE (2018) A model for studying the energetics of sustained high frequency firing. PLoS ONE 13(4): e0196508. https://doi.org/10.1371/journal.pone.0196508

Editor: Vladimir E. Bondarenko, Georgia State University, UNITED STATES

Received: November 6, 2017

Accepted: April 13, 2018

Published: April 30, 2018

Data Availability Statement: The paper is strictly computational. Parameters used with the equations are given in Table 1.

Funding: BJ and JEL thank the Natural Sciences and Engineering Research Council of Canada (http://www.nserc-crsng.gc.ca) for funding. MRM acknowledges support from the National Science Foundation (https://www.nsf.gov/) (grants IOS1257580 and IOS1350753). CEM acknowledges support from the Ottawa Hospital Research Institute (www.ohri.ca). The funders had no role in study design, data collection and

Abstract

Regulating membrane potential and synaptic function contributes significantly to the energetic costs of brain signaling, but the relative costs of action potentials (APs) and synaptic transmission during high-frequency firing are unknown. The continuous high-frequency (200-600Hz) electric organ discharge (EOD) of *Eigenmannia*, a weakly electric fish, underlies its electrosensing and communication. EODs reflect APs fired by the muscle-derived electrocytes of the electric organ (EO). Cholinergic synapses at the excitable posterior membranes of the elongated electrocytes control AP frequency. Based on whole-fish O_2 consumption, ATP demand per EOD-linked AP increases exponentially with AP frequency. Continual EOD-AP generation implies first, that ion homeostatic processes reliably counteract any dissipation of posterior membrane E_{Na} and E_K and second that high frequency synaptic activation is reliably supported. Both of these processes require energy. To facilitate an exploration of the expected energy demands of each, we modify a previous excitability model and include synaptic currents able to drive APs at frequencies as high as 600 Hz. Synaptic stimuli are modeled as pulsatile cation conductance changes, with or without a small (sustained) background conductance. Over the full species range of EOD frequencies (200–600 Hz) we calculate frequency-dependent "Na^+-entry budgets" for an electrocyte AP as a surrogate for required $3Na^+/2K^+$-ATPase activity. We find that the cost per AP of maintaining constant-amplitude APs increases nonlinearly with frequency, whereas the cost per AP for synaptic input current is essentially constant. This predicts that Na^+ channel density should correlate positively with EOD frequency, whereas AChR density should be the same across fish. Importantly, calculated costs (inferred from Na^+-entry through Nav and ACh channels) for electrocyte APs as frequencies rise are much less than expected from published whole-fish EOD-linked O_2 consumption. For APs at increasingly high frequencies, we suggest that EOD-related costs external to electrocytes (including packaging of synaptic transmitter) substantially exceed the direct cost of electrocyte ion homeostasis.

analysis, decision to publish, or preparation of the manuscript.

Competing interests: The authors have declared that no competing interests exist.

Introduction

Analysis of mammalian brain energetics identifies electrical signaling as the major consumer of ATP with molecular processes underlying synaptic transmission incurring the highest costs [1–3]. For brain, the costs of low frequency electrical signalling arising from various aspects of ion homeostasis have been analyzed and summarized (see Table 2A in Ref. [3]). Changes in ion concentrations due to synaptic inputs and action potentials (APs) are reversed by the action of energy-consuming ion pumps. This direct link allows energy consumption to be estimated from Na^+-entry [1, 4] which drives the $3Na^+/2K^+$-ATPase activity (at 1 ATP/3 Na^+ expelled). Under the low-firing frequency conditions (4 Hz) typical of mammalian cortex, Na^+ (and Ca^{+2}) entry through postsynaptic receptor channels is estimated to be much larger than that through AP-related voltage-dependent Na+ (Nav) channels. Synaptic processes are thus thought to dominate energetic costs in these conditions, but whether this is the case for other firing regimes is not known.

The weakly electric fish, *Eigenmannia*, generates a high-frequency electric organ discharge (EOD) for electric sensing (**Fig 1A**). The electric organ (EO), an array of electrocytes derived from skeletal muscle (but with no contractile machinery), is a relatively simple and homogeneous excitable cell tissue. Electrocytes are posteriorly innervated syncytial cells, each ~1 mm long, with capillary beds at either end. EOD frequency is set centrally and conveyed to electrocytes via cholinergic nerve terminals at their posterior membranes. Regular and unremitting synaptic triggering of action potentials (APs) in synchronously firing electrocytes produces an externally detectable EOD at an individual-specific frequency within in the species range (200–600 Hz).

For brain energetics in general, functional magnetic resonance imaging reports on localized regions of elevated neural activity via local/temporal variations in O_2-rich blood flow [7, 8]. However, tissue complexity and low spatial resolution impedes the study of discrete excitable cell activities, making interpretation of images problematic [9]. *Eigenmannia* is special in that whole-animal O_2 consumption (and thence ATP usage) can be linked to a uniform unremitting excitability process, the EOD [9]. Like skeletal muscle fibers (from which electrocytes derive), the EOD producing electrocytes have cholinergic synapses and capillaries that ramify extensively with fine invaginations of the plasma membrane [5, 10, 11]. Being non-contractile, electrocytes are physiologically simpler than skeletal muscle. It seems worth exploiting this simplicity to work out how cyto- and tissue architecture interact with the molecular machinery of excitability to so reliably yield the EOD. Although the spatiotemporal variations in electric potential surrounding the intact discharging fish has been well-described [12, 13], it is not established where and for which specific processes ATP is used to maintain this oscillating discharge. Models are required to describe the underlying cellular and tissue level processes and then predict the known whole animal EOD pattern.

Monitoring EODs *in vivo* allows for precise quantitation of various aspects of *Eigenmannia*'s high-frequency excitability [12, 14]. Exploiting this, Lewis et al [6] found that the inferred ATP consumption per EOD-linked AP is not constant across all frequencies as generally assumed [1, 15], but instead increases exponentially with EOD frequency (see **Fig 1B**). This indicates that the energetics of high frequency excitability need more attention. Given the potential utility of *Eigenmannia* as a tool, a sound mathematical model for its EOD-producing machinery is required. Building on a previously-proposed model of a single electrocyte [16], we propose a new model, "Epm", that includes synaptic input and is more robustly excitable. Over the range 200–600 Hz, Epm predicts that ATP consumption per AP is not constant. Using Epm to explore the source of Na^+-entry at various frequencies leads to the prediction that Nav channel density but not AChR channel density should increase as a function of AP

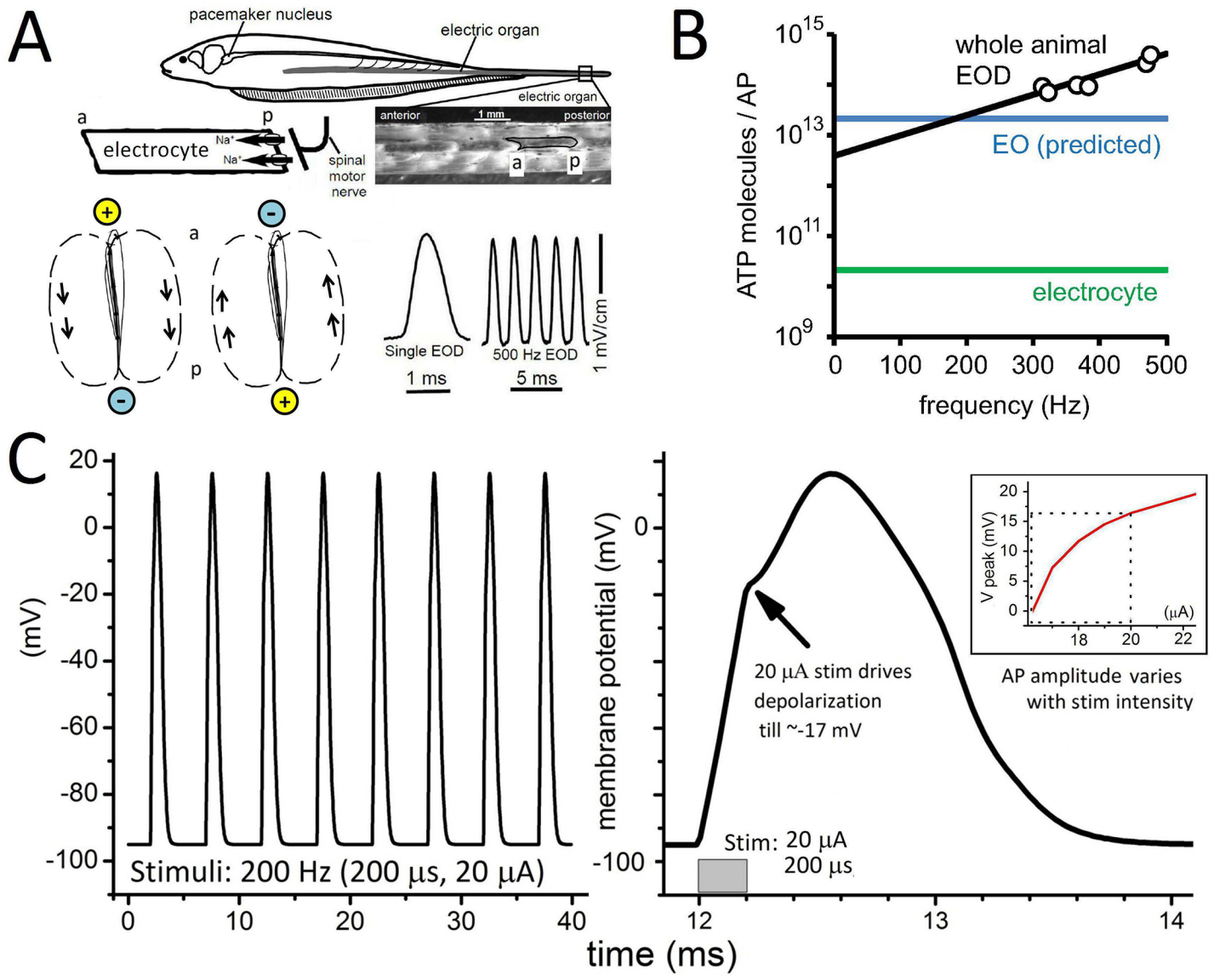

Fig 1. Background information. A. (modified from Ref. [5]) *Eigenmannia*, showing the electric organ (EO) location and the anterior(a)/posterior(p) disposition of its constituent electrocytes, each innervated posteriorly by a (central pacemaker driven) cholinergic electromotor neuron synapse (i.e., electroplaque). Due to the rapidly alternating head-positive/head-negative polarization from the continual EO discharge (EOD), the fish in its aqueous medium approximates an oscillating dipole [6]. **B.** Plot from Ref. [6], summarizing the unexpected observation (calculated from whole fish O_2 consumption data linked to *Eigenmannia* EOD frequencies) that APs cost more as AP frequency increases. **C**. Left, an MKZ-simulated AP train (gNa_{max} = 700 µS) driven by pulsatile I_{clamp} as labeled, and right, one AP with the time scale expanded to make evident the apparent threshold region (~-17 mV) (inset: V_{peak} as a function of I_{stim}).

https://doi.org/10.1371/journal.pone.0196508.g001

(i.e. EOD) frequency. In the context of the EOD-linked O_2-consumption reported by Lewis et al [6], these results strongly suggest that the electrocytes themselves are energetically efficient devices and that a greater fraction of global cost of EOD production can be attributed to pre-synaptic processes (e.g., packaging and recycling of ACh quanta) than to supporting electrocyte ion homeostasis. Comparable predictions have been made, interestingly, regarding the relative costs incurred for synaptic transmission versus electrical propagation by in situ mammalian central neurons [3, 4, 17].

Methods

Limitations of a previous model

Since *Eigenmannia* electrocytes' continual APs demand narrowly-maintained equilibrium potentials (E_K and E_{Na}), homeostatic processes evidently succeed in minimizing fluctuations of [Na^+] and [K^+] close to the AP-generating membrane. A previously developed excitability model for isolated electrocytes (termed here, "MKZ" for Markham, Kaczmarek, Zakon, 2013) [16] depicts a system that is quiescent until stimulated by intracellular current injection (I_{clamp}). This model does not include an explicit Na^+/K^+ pump so initially we intended to incorporate one and explore E_K and E_{Na} stability for APs at frequencies over the species range (200–600 Hz). Because pump function is electrogenic, a key system requirement is to stabilize membrane potential (V_m) at the resting value (V_{rest}) of the unstimulated excitable system. Stabilization is accomplished via Na^+ and K^+ leaks of appropriate magnitudes [18] This however renders MKZ inexcitable because the very small V_{rest}-E_K necessitates an enormous K^+-specific leak to counter pump electrogenicity and this makes V_m ultra-stable near V_{rest}.

Fig 1C shows MKZ APs during a 200 Hz stimulus train (same parameters as in Fig 3A in Ref. [16]); an expanded AP (right panel) reveals that the regenerative ΔV_m covers ~35 mV (from ~-17 mV to +17 mV) and that V_{peak} depends strongly on I_{stim} (see inset) and so is not strictly all-or-none. Excitability that depends strongly on large amplitude stimuli in this way seems ill-suited for *Eigenmannia*'s robust high frequency EOD output.

The MKZ model assumes an isopotential electrocyte in which the membrane current ($I_{membrane}$) charges and discharges 50 nF of membrane capacitance. While space-clamp (isopotential) is necessary for electrocyte voltage clamp recordings, electrocytes are in general not isopotential in situ as Na^+-entry occurs exclusively via Nav channels at the innervated posterior membrane, located ~1 mm distant from the anterior membrane, which is channel-rich but inexcitable [5] In *Sternopygus* [19] and presumably *Eigenmannia* current flow across the intracellular series resistance results in an anterior-posterior potential difference of several tens of millivolts.

An excitability model applicable to EODs should mimic AP features of healthy electrocytes under current clamp (I_{clamp}) where AP thresholds are close to -45 mV during tonic firing when evoked by a constant current stimulus (40 ms) [16]. Applying constant current stimuli to the MKZ model (rather than the much larger 0.2 ms current pulses used by Lewis et al. [6] however, elicits only one high threshold AP and after a damped oscillation, the V_m settles to a depolarized plateau. Inspection of Fig 1C shows that for modeled MKZ-APs elicited by a 0.2 ms pulse, most of the depolarization (~60 mV of the total AP voltage excursion) is accomplished not by I_{Na} but by the large injected current. The model developed in the next sections, Epm, addresses this and several other limitations of the MKZ model.

The new excitability model (Epm) considers only the posterior excitable membrane. Demand on the Na^+/K^+ pump resulting from APs is inferred from net Na^+-entry across this membrane. No specific inference is made about where and how pump electrogenicity is managed in the electrocyte. This issue, plus anterior membrane contributions to high-frequency EODs and ion homeostasis will be addressed in later work.

APs are spikes in the transmembrane potential, V (or V_m), and are solutions of the equation:

$$C\frac{dV}{dt} = -I_{NaT} - I_{NaP} - I_K - I_L + I_{stim}, \quad (1)$$

where C is the capacitance of the electrocyte membrane, I_{NaT} (transient) and I_{NaP} (persistent) are the currents through Nav channels, I_K, the current through Kv channels, I_L, the generic

leak current and I_{stim}, the stimulus current initiating the APs. We only show the currents included in the Epm model. The reader is referred to [16] and [6] for other currents in the MKZ model.

$$I_{NaT} = \mathrm{gNa}_{\max} m^3 h(1-\gamma)(V - E_{Na}), \tag{2}$$

$$I_{NaP} = \mathrm{gNa}_{\max} m^3 \gamma (V - E_{Na}), \tag{3}$$

$$I_K = \mathrm{gK}_{\max} n^4 (V - E_K), \tag{4}$$

where the kinetic variables $j = m$, h, and n obey the equation:

$$\frac{dj}{dt} = \alpha_j(1-j) - \beta_j j, \tag{5}$$

while I_L is given by:

$$I_L = g_L(V - E_L), \tag{6}$$

and I_{stim} can flow either through a current clamp electrode or through post-synaptic cation channels, as presented in the next section. Values for parameters in the models MKZ and Epm appear in **Table 1**.

Further details on the above currents are discussed in the following sections starting with the cation channel version of I_{stim}.

A post-synaptic cation conductance for Epm

EOD frequency-dependent O_2 consumption [6] pertains to the *in vivo* situation, with APs triggered by post-synaptic current through acetylcholine receptor channels (AChRs). In Epm, an electro-diffusion description of ion permeation through this class of channel allows for separate tallying of Na^+ and K^+ fluxes.

$$I_{stim} = \mathrm{syn}_{clamp}(t)(I_{AChR(Na)} + I_{AChR(K)}) \tag{7}$$

with:

$$I_{AChR(X)} = P_X F z \left(\frac{zFV/RT}{1 - e^{-zFV/RT}}\right)[[X]_{in} - [X]_{out} e^{-zFV/RT}], \tag{8}$$

where X is either Na^+ or K^+, the two ions that are permeant through the AChR channels, F is the Faraday constant, R the gas constant, V the transmembrane potential and z the valence of the ions. The ratio of the permeabilities P_K/P_{Na} is 1.11 as given in **Table 1** and the absolute value of P_{Na} was chosen to yield an appropriate-sized stimulus for the modeled posterior membrane. In the standard pulsatile stimulation used here the maximum value of $\mathrm{syn}_{\mathrm{clamp}}(t)$ is 1; higher values will imply correspondingly higher densities of activatable AChRs. In what follows $\mathrm{syn}_{\mathrm{clamp}}W$ or $\mathrm{syn}_{\mathrm{clamo}}\mathrm{W}_{0\mathrm{Hz}}$ will indicate a constant "cation permeability clamp" of magnitude W (for example $\mathrm{syn}_{\mathrm{clamp}}0.5$ means that $\mathrm{syn}_{\mathrm{clamp}}(t) = 0.5$).

For *Sternopygus* [20] and *Electrophorus* [21] excitatory postsynaptic potentials (epsp) and miniature post-synaptic currents at the "electroplax" (mepsc), respectively, have been recorded. *Electrophorus* miniatures are slower than those at frog endplates [21], nevertheless, during predatory strikes, the electric eel can produce brief EOD bursts at ~400 Hz [22] (mechanistic details are unknown). *Eigenmannia* EODs demand continuous APs at up to 600 Hz [23] presenting an even more extreme challenge, assuming the electrocytes fire 1:1 with the

Table 1. Kinetic constants for the MKZ and Epm models. MKZ parameters are from Ref [6]. Listed gNa_{max} values are for the 200 Hz case. For Epm, the gNa_{max} values used for other frequencies are discussed in the Section **Frequency-dependent cost per AP**.

	MKZ	Epm
g_L	0.76 μS	5 μS
C	50 nF	50 nF
Equilibrium and reversal potential		$[Na]_i$ = 1.35 mM
		$[Na]_o$ = 120 mM
		$[K]_i$ = 89 mM
		$[K]_o$ = 2.16 mM
E_{Na}	50 mV	55 mV
E_K	-95 mV	-94 mV
E_L	-93 mV	E_K
V_{rev}(AChR)	n.a.	2.18 mV
***$g_{Na}(V)$* Na channels**		
gNa_{max}	700 μS	700 μS
γ	0.1	0.02
$k_{\alpha m}$	7.6 ms^{-1}	8.03 ms^{-1}
$k_{\beta m}$	0.6894 ms^{-1}	0.2195 ms^{-1}
$\eta_{\alpha m}$	0.0037 mV^{-1}	0.0037 mV^{-1}
$\eta_{\beta m}$	-0.0763 mV^{-1}	-0.0763 mV^{-1}
$k_{\alpha h}$	0.00165 ms^{-1}	0.02247 ms^{-1}
$k_{\beta h}$	0.993 ms^{-1}	n.a., HH type
$\eta_{\alpha h}$	-0.1656 mV^{-1}	-0.06802 mV^{-1}
$\eta_{\beta h}$	-0.0056 mV^{-1}	n.a. (see *)
***$g_K(V)$* delayed rectifier**		
gK_{max}	2000 μS	2000 μS
$k_{\alpha n}$	1.209 ms^{-1}	2.135 ms^{-1}
$k_{\beta n}$	0.4448 ms^{-1}	0.3524 ms^{-1}
$\eta_{\alpha n}$	0.00948 mV^{-1}	0.03792 mV^{-1}
$\eta_{\beta n}$	-0.01552 mV^{-1}	-0.01552 mV^{-1}
a *	2.5 mM^{-1} ms^{-1} nA^{-1}	n.a.
a' *	12.5 mM^{-1} ms^{-1}	n.a.
b *	0.5 ms^{-1}	n.a.
k_f *	10 mM^{-1} ms^{-1}	n.a.
k_b *	2.0 ms^{-1}	n.a.
Inward rectifier	(g_{KIR})	
g_R	300 μS	0
η_R	0.22 mV^{-1}	n.a.
AChR (post-synaptic)		
P_{Na}	n.a.	0.00016 mm^3/s
P_K	n.a.	1.11 P_{Na}

* In the MKZ model the impact of intracellular Na on the Kv conductance is modeled through a parameter *s* as described in Eqs 10 and 11 in Ref. [6] and on p. 1715 of Ref. [16]. The * parameters characterize the equations governing the kinetics of *s* which turns out to have no effect on Kv conductance because, after 1 ms, *s* deviates very little from unity.

https://doi.org/10.1371/journal.pone.0196508.t001

EOD frequency [14, 19]. Even a subset of exceptionally short-lived events recorded from *Torpedo* electroplax (an elasmobranch, not a teleost) [24] or the fast rising endplate currents

reported for lizard muscle [25] would be too slow overall. We model high frequency synaptic AChR activation using a pulsatile syn_{clamp} stimulus that could operate effectively up to just beyond 600 Hz. Because such short-lived stimuli are strictly conjectural, we also consider steady-state (0 Hz) syn_{clamp}, and mixed stimuli (i.e. pulsatile atop some background AChR activation).

gNa(V) characteristics for Epm

The voltage dependent kinetic variables α_j and β_j in Epm (and MKZ) have the form $\alpha_j = k_{\alpha j} e^{\eta_{\alpha j} V}$ or $\beta_j = k_{\beta j} e^{\eta_{\beta j} V}$ where the pre-factors $k_{\alpha j}$ and $k_{\beta j}$, and the exponential factors $\eta_{\alpha j}$ and $\eta_{\beta j}$ are given in Table 1. The one exception is the kinetic variable β_h which describes the rate of inactivation. In Epm it has the functional form used by Hodgkin and Huxley for squid axon:

$$\beta_h = \frac{3.33}{\exp(-(V+30)/9) + 1.0}. \quad (9)$$

For MKZ and Epm, Fig 2 plots the characteristics in Hodgkin-Huxley terms [26, 27] of the voltage-gated conductances. In MKZ the $m^3(V)$ midpoint is -13 mV (Fig 2). The $G/G_{max}(V)$ reported for *Eigenmannia* electrocytes is, however, -37 mV (Fig 3 of Markham et al., 2013 [16]); for Epm the choice of prefactor $k_{\alpha m}$ set the midpoint of $m^3(V)$ at -28mV (see Fig 2). For the rate of recovery from inactivation (forward inactivation rate) α_h (V) (**Eq (3)**), the exponential factor $\eta_{\alpha h}$ has the value used by Cannon and colleagues (Table 1 in [28]; originally from

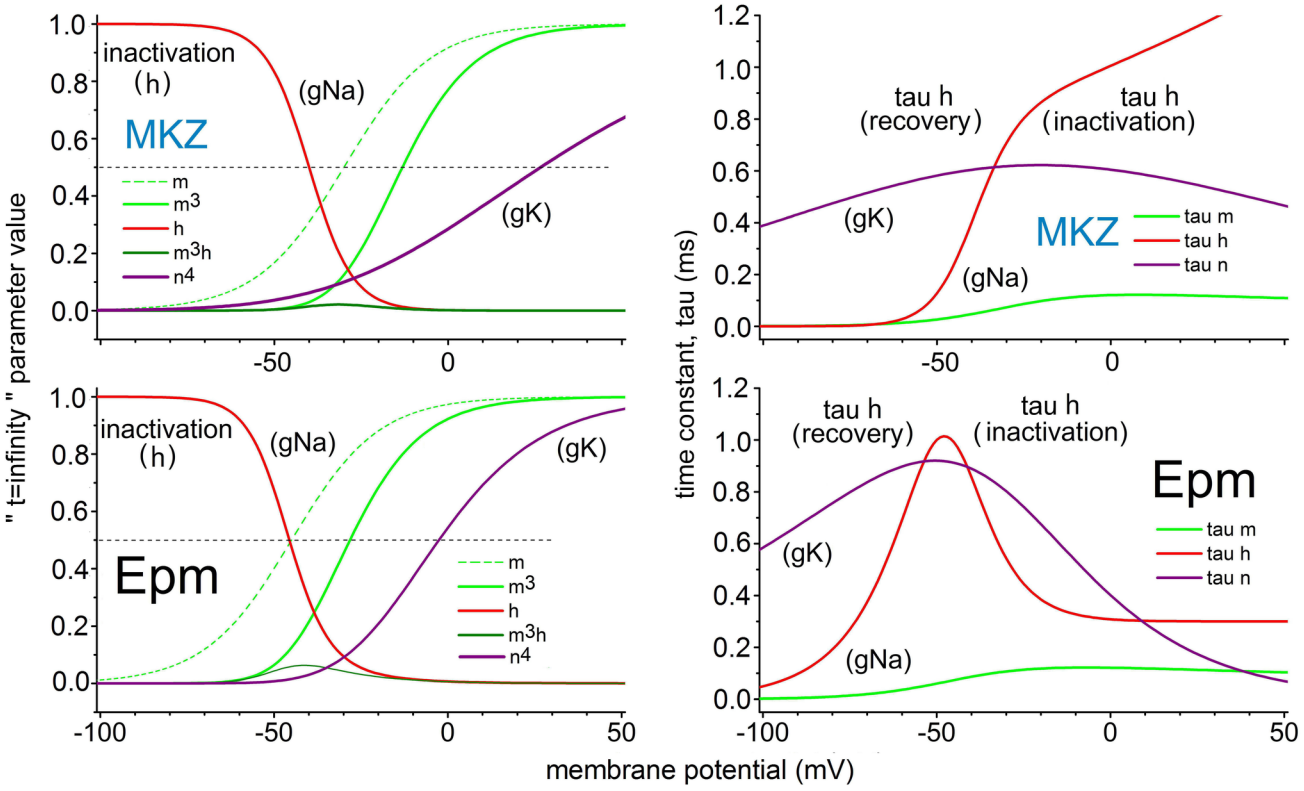

Fig 2. Graphical comparison of the V-gated conductances of MKZ and Epm. The plots are generated using parameters in Table 1. Left: equilibrium (i.e., $t \to \infty$) values of the Hodgkin-Huxley parameters. As labeled, gNa and gK are proportional to m^3 and n^4 respectively, and, h is proportional to the availability (or inactivation status) of the Na conductance. Right: time constants for these processes (see text for more explanation). For tau_h (V) curves, the voltage regions dominated by the recovery and the inactivation processes are indicated.

https://doi.org/10.1371/journal.pone.0196508.g002

Pappone [29] for mammalian skeletal muscle).

$$\alpha_h = k_{\alpha h} e^{\eta_{\alpha h} V} \quad (10)$$

The prefactor $k_{\alpha h}$ was adjusted to yield a robust window conductance (see m^3h for Epm in Fig 2). Our choice of the backward inactivation rate $\beta_h(V)$(**Eq (9)**) ensures the fast development of the APs and a very brief refractory period. We note that while in the Hodgkin-Huxley papers, τ_h (for the squid axon) converges to 1 ms for large depolarizations, the parameters here make τ_h go asymptotically to 0.3 ms as reported by Shenkel and Sigworth [30] (see their Fig 3B up to ~+20 mV and their Fig 8C) for *Electrophorus* electrocytes. Epm inactivation kinetics, unlike in MKZ, conform to a standard Hodgkin-Huxley form (see τ_h plots, **Fig 2**). In the electric fish *Electrophorus*, *Sternopygus*, and *Eigenmannia*, τ_h begins to increase at large depolarizations [16, 20, 30], but because the voltages in question are beyond the physiological range, this feature was not included in the model.

Epm retains a simple persistent gNa(V) with the same activation kinetics as for the transient gNa(V) and no inactivation (see Eq (3). It has a lower magnitude than MKZ, i.e., $\gamma = 0.02$ in Epm versus 0.1 in MKZ (**Table 1**)).

K conductances for Epm

It was formerly thought that Na^+-activated I_K (I_{KNa}) and persistent I_{Na} recorded from *Eigenmannia* electrocytes form an interacting pair [16], but subsequent immunocytochemical evidence located K_{Na} and Nav channel proteins exclusively to anterior and posterior membranes, respectively [5]. While Epm retains a (diminished) persistent gNa, it does not include the gK_{Na}. Moreover, its description in MKZ as a "Na^+-activated gK" notwithstanding, this conductance operates as a classic delayed rectifier under the modelled conditions. Its modulation by *s*, the non-dimensional parameter sensitive to $[Na^+]_{intracellular}$ (see *Materials and Methods* section in [16]), is inconsequential since the value of *s* converges within ~ 1 ms to unity. Additionally, $\Delta[Na^+]_{intracellular}$ had no impact on E_{Na} which is held constant in that model. Thus with or without the MKZ "*Na*-modulation" (asterisks (*) in **Table 1**), MKZ APs (e.g. **Fig 1C**) are identical. Accordingly, additional, experimental and computational, efforts are needed to resolve the functional contributions of gK_{Na} in *Eigenmannia* electrocytes.

Eigenmannia electrocytes have an inwardly rectifying *gK* [16] whose normal operating range is sufficiently hyperpolarized that even if some were present at the posterior membrane, it would neither contribute to nor interfere with excitability. Skeletal muscle t-tubular membrane [31] has abundant Kir2 protein. Kir2 mRNA transcripts have been detected in *Eigenmannia* electrocytes [32], but these channels have not to date been localized in the electrocyte, whereas Kir6 protein (an ATP-sensitive *gIR*) is expressed only on the anterior electrocyte membrane [5]. Thus, MKZ included *gIR*, but Epm does not.

Although a delayed rectifier current is evident in *Sternopygus* [20], a Na^+-independent delayed rectifier K^+ current is not present in *Eigenmannia* electrocytes [16]. However, without a *gK(V)*, high frequency excitability fails. It has been suggested for *Electrophorus* that "the membrane potential is repolarized by Na^+ channel inactivation, and from the conductance of Cl^- and K^+ through leak channels" (p. 230 in [33]), in other words, without a delayed rectifier. This seems untenable for *Eigenmannia* whose electrocytes must fire from 200 Hz up to 600 Hz. With no delayed rectifier, the 50 nF membrane would need an RC time constant of ~1 ms to repolarize by ~ -100 mV (+20 mV to -80 mV). This requires a leak (g_K and/or g_{Cl}) of 50 μS (for reference $g_{Leak} = 0.76$ μS in MKZ) that would render the membrane inexcitable unless gNa_{max} was massive. For Epm, we retained the $C_m = 50$ nF of MKZ, thus requiring the inclusion of a

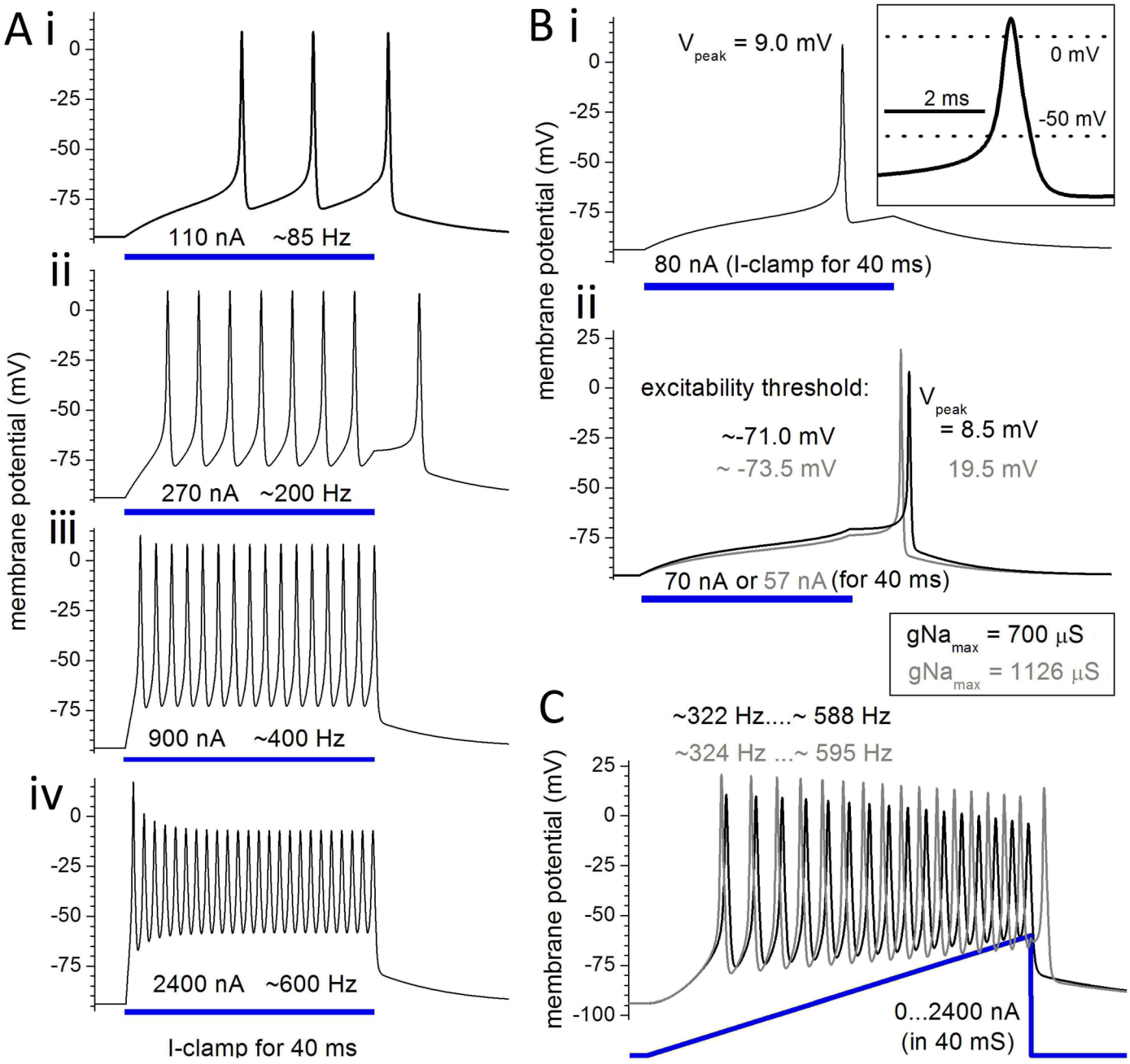

Fig 3. Sustained step and ramp I_{clamp} stimulation of Epm. Standard gNa_{max} (700 µS) is used unless otherwise specified, I_{stim} as labeled, other parameters as in Table 1. See text for further explanation.

https://doi.org/10.1371/journal.pone.0196508.g003

delayed rectifier K^+ conductance in Epm. For this delayed rectifier we retained the MKZ gK_{max} of 2000 µS. With these constants, use of gNa_{max} = 700 µS gives a reasonable overshooting V_{peak} value for APs at the low end of the EOD range (200 Hz) (e.g. use of at gNa_{max} = 400 µS at 200 Hz gives V_{peak} = ~0 mV). Accordingly, for Epm, gNa_{max} = 700 µS was made the "standard" for APs at 200 Hz (Table 1).

Having settled on the parameters for gNa(V) and established the need for a delayed rectifier (gK(V)) within Epm, it was necessary to design the latter to allow for APs up to 600 Hz. We

assumed that gK(V), when activating, should not interfere with the depolarizing I_{Na}, but instead should develop rapidly just after the AP has overshot 0 mV, and thus drive repolarization. An $I_K(V)$ that activates in this manner would be consistent with an impedance analysis of *Sternopygus* electrocyte APs (see Fig 28 in [19] or Fig 41 in [34]). That analysis shows that after a conductance associated with rapid depolarization falls rapidly, another conductance grows rapidly. These characteristics were achieved via the Epm gK(V) parameters listed in **Table 1**, which result in a gK activation curve ($n^4(V)$ in **Fig 2**) whose midpoint is -2.6 mV and whose slope is 0.017 mV^{-1} (equivalent to 14.7 mV per e-fold). Interestingly, these values are very similar to those reported for a skeletal muscle gK(V) (Kv3.4, Fig 2C of [35]).

Results

Epm responses to constant current stimulation

For Epm, a sustained constant current stimulation (I_{stim}) (40 ms, as per *Eigenmannia* I-clamp experiments: Fig 1 of [16]) yields trains of overshooting, all-or-none, strongly regenerative APs that, depending on I_{stim} intensity, fire at frequencies from below to above the species EOD range (200–600 Hz) (**Fig 3Ai-iv**). Even after I_{stim} ends Epm can fire a full-amplitude AP before settling to V_{rest} (**Fig 3Aii**). Note that as I_{stim} is increased the frequencies near 600 Hz (**Fig 3Aiv**) can be attained but at diminished AP amplitude. Another indicator that Epm is robustly excitable is seen in **Fig 3B**, where an AP fires as the membrane depolarizes past ~-70 mV during a small I_{stim} (**Fig Bi**) or even after, provided the I_{stim} value is extremely close to threshold (**Fig Bii**). For larger values of gNa_{max} (grey in **Fig 3Bii**), minor quantitative differences in AP characteristics are evident. The model electrocyte would be even more prone to fire in the presence of the current noise typical during synaptic activation. The Epm system exhibits "Class 1 excitability" (pp 219–221 of [36]); APs of arbitrarily low frequency can be triggered, depending on the strength and duration of I_{stim}.

In **Fig 3C**, firing is elicited by an I_{stim} ramp of 40 ms duration going to a maximum of 2400 nA, resulting in frequencies that begin near ~320 Hz and increase to ~600 Hz (note the progressively diminishing AP amplitude for both gNa_{max} = 700 and 1126 μS). The initial frequency depends on ramp steepness (the shallower the slope the lower the initial frequency, not shown) and the maximal frequency, which is set by channel kinetics, depends only on I_{stim} magnitude.

Reduced V_{peak} values at high frequencies (e.g., see **Fig 3Aiv and 3C**) point to a question addressed in the next section and raised previously [6], namely, is there a need for higher Nav channel density to sustain higher frequency APs? For *Eigenmannia* individuals this would correspond to a positive correlation between EOD frequency and Nav channel density.

Epm responses to pulsatile synaptic current stimulation

We assume that each electrocyte AP is triggered by a brief pulsatile AChR-mediated post-synaptic current intense enough to yield full-amplitude APs at frequencies up to 600 Hz (see **Fig 4**). The shape of this standard stimulus ($syn_{clamp}1$) is based on synaptic currents in Torpedo [24] and lizard [25] see **Fig 4** legend and **Table 1**.

Fig 5A plots the membrane potential and underlying variables for a single Epm AP in a 200 Hz train. During the stimulus (top) net Na^+ influx (I_{Na}) is substantial while I_K is minimal (E_K is near V_{rest}). Because the stimulus ends before $V_m(t)$ reaches the V_{rev} for AChRs (+2.2mV) both I_K and I_{Na} components of the syn_{clamp} remain unidirectional. As in I-clamped *Eigenmannia* electrocytes [16] the AP shows an apparent threshold region near -45 mV (**Fig 5A**). The AP peaks at ~13 mV (for computations V_{peak} = +12.86 mV), a value used in connection with $syn_{clamp}1$ as the "standard" AP-amplitude. Early $I_{Na}(V,t)$ is unopposed but the rapid-onset of $I_K(V,t)$ then drives AP repolarization in co-operation with gNa inactivation. Recovery from

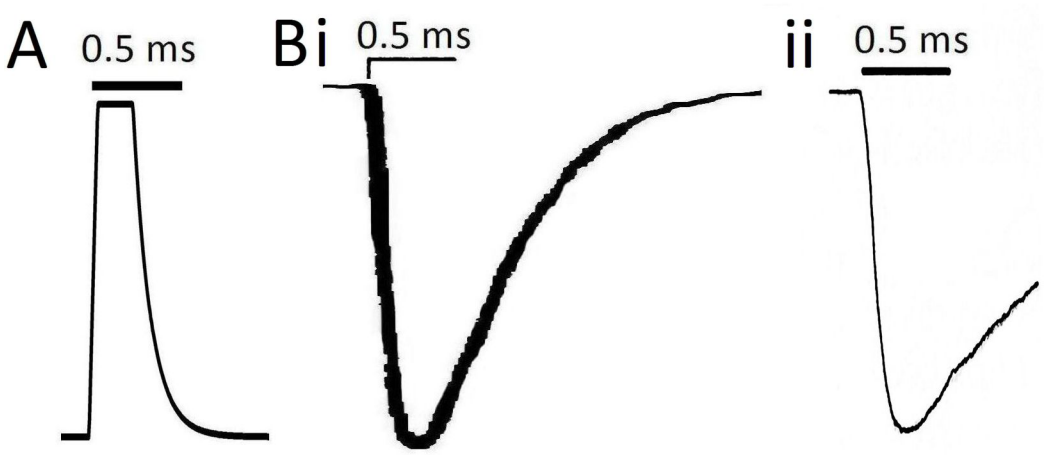

Fig 4. A. The standard pulsatile stimulus shape syn_{clamp} (t) used in Epm has 3 segments: a linear rise for 0.05 ms, a plateau for 0.200 ms and an exponential decay to zero (specifically the segments are: $syn_{clamp}1.0$ (t) = t/0.05 (t<0.05); 1 (0.05<t<0.25); and exp[-(t-0.25)/0.1] (t>0.25), t in ms)). **Bi.** For comparison, a depiction of the fastest cholinergic post-synaptic event we found in the literature for electroplaques, shown at the same time scale as the standard pulsatile stimulus in A. The miniature electroplaque current (mepc) depicted exemplifies a fast subclass of of mepc recorded in relatively intact *Torpedo* electroplaques [24]. **Bii** depicts the average time course of mepcs measured from lizard intercostal muscle [25]. The pulsatile stimulus used in Epm is speedier in all respects than these mepcs. Whereas a mepc results from a quantal release event that would be insufficient to stimulate an entire electroplaque, the syn_{clamp} stimuli of Epm must provide sufficient "ACh-activated" I_{cation} at the *Eigenmannia* electroplaque to rapidly depolarize to threshold 50 nF of post-synaptic membrane. Thus, 1:1 triggering (1 electromotor neuron AP: 1 electrocyte AP) is assumed, but how it would be achieved at up to 600 Hz in vivo is not understood.

https://doi.org/10.1371/journal.pone.0196508.g004

inactivation is almost complete ~1 ms after V_{peak}. As a result Epm APs at 200 Hz are indistinguishable from APs at lower frequencies.

To maintain a constant V_{peak} at higher frequencies, gNa_{max} values must increase (as with MKZ; [6]). Fig 5B compares model variables at 200 Hz and 600 Hz with gNa_{max} kept at 700 μS for both frequencies (left) or with gNa_{max} increased to 1126 μS for the 600 Hz APs (right). These values plus those needed for intervening frequencies are also indicated as plot labels in Fig 6B**.** The bottom panels of Fig 5B show that Na^+ entry at 200 Hz vs 600 Hz is unaffected if the AP amplitude (top panels) is allowed to fall (left) but increases markedly if gNa_{max} is adjusted to attain the standard V_{peak} (top right). The middle panels reveal that the voltage-gated channels' activation kinetics are not limiting here; the rise and fall of parameters m^3 and n^4 (which reflect open-gNa and open-gK) is rapid enough at both 200 and 600 Hz (middle panels).

Because gK_{max} was held constant across frequencies while gNa_{max} was increased, the AP depolarization rate and hence the speed of gNa activation and inactivation onset increases with frequency. The limiting factor for maintaining full amplitude APs is recovery from inactivation. The middle panels of Fig 5B show that *h* (sodium channel availability or inactivation status) at 600 Hz has insufficient time to return to unity after each AP; at 600 Hz *h* barely reaches 0.8 before the next AP. Failure to fully recover from inactivation underlies the requirement for increased gNa_{max} at 600 Hz. Thus, while overall AP shapes differ only subtly between 200 and 600 Hz, the faster rise to threshold (and then to peak) at 600 Hz is not inconsequential. It is possible only because of the augmented Na^+-entry (Fig 5B bottom panel, right).

Frequency-dependent cost per AP

Thus, in the Epm model, the increased gNa_{max} needed to sustain APs at full amplitude with increasing frequency predicts that the cost/AP (Hz) will rise. Fig 6A illustrates a few APs from

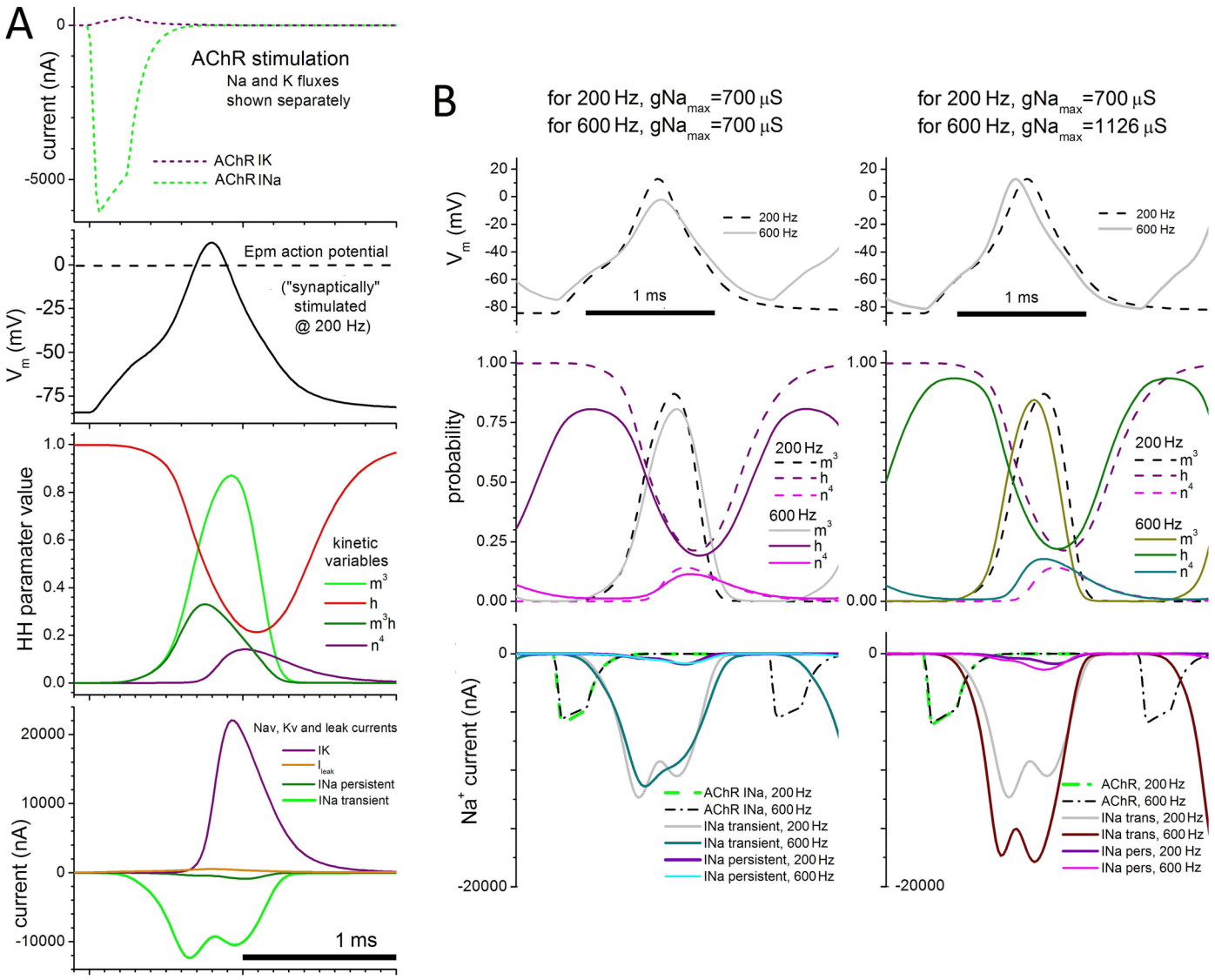

Fig 5. Epm-simulated APs stimulated by pulsatile synaptic current. A. One AP from a 200 Hz AP train (stimulus: $syn_{clamp}1.0_{200Hz}$) with gNa_{max} = 700 µS. **B.** For gNa_{max} values as labeled, APs from trains with stimulus $syn_{clamp}1.0_{200Hz}$ or $syn_{clamp}1.0_{600Hz}$. First column, gNa_{max} = 700 µS; second column, for $syn_{clamp}1.0_{600Hz}$, gNa_{max} is raised to 1126 µS to bring V_{peak} to 13 mV. See text for further explanation.

https://doi.org/10.1371/journal.pone.0196508.g005

trains of Epm APs elicited by pulsatile syn_{clamp} at 200 Hz, 600 Hz, and the unphysiologically rapid 700 Hz. Such APs are used to calculate Na^+-entry (trains of at least 20 APs were generated), which is a proxy for energetic cost/AP. Given sufficient gNa_{max}, AP trains are attainable up to ~650 Hz in Epm, whereafter irregularities appear (e.g., see 700 Hz in Fig 6A).

The upper panel of Fig 6B combines Na^+ entry through V-gated (Nav) and synaptic (AChR) channels. The cost/AP increases nonlinearly over this range of frequencies. However, separating the synaptic cost/AP(Hz) reveals that the cost of synaptically stimulating APs is essentially constant. Hence, the non-linearity in cost/Hz can be ascribed to Nav currents. Since our initial choice of gNa_{max} = 700 µS at 200 Hz may seem arbitrary, we also ran calculations with gNa_{max} = 900 µS. Briefly, this increases V_{peak} to ~18 mV, which means larger values of Na^+ entry for the gNa, but nearly unchanged synaptic costs.

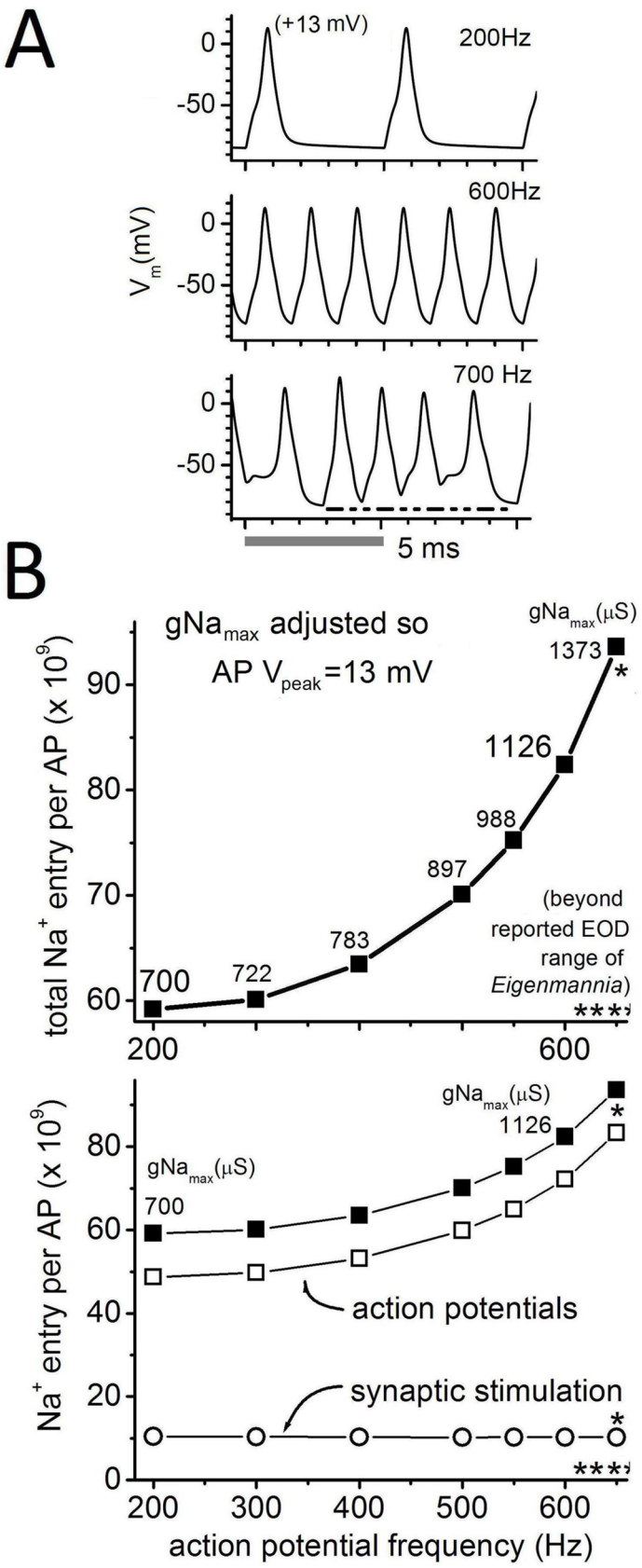
A
(+13 mV)
200Hz
600Hz
700 Hz
0
-50
V_m (mV)
5 ms
B
gNa_{max} adjusted so
AP V_{peak}=13 mV
gNa_{max}(μS)
1373
1126
988
897
783
722
700
(beyond reported EOD range of *Eigenmannia*)
total Na^+ entry per AP (x 10^9)
Na^+ entry per AP (x 10^9)
action potentials
synaptic stimulation
action potential frequency (Hz)

Fig 6. Cost of Epm APs at different AP frequencies based on Na^+-entry. A. Illustrated are APs firing at 200 Hz and 600 Hz and then failing at 700 Hz which, however, exceeds the biological range of *Eigenmannia* (700 Hz stimulation elicits APs with irregular amplitudes and timing). For all frequencies the pulsatile stimulus amplitude was $syn_{clamp}1.0$ and gNa_{max} was adjusted to yield V_{peak} = 13 mV. To calculate Na^+-entry (= the time integral of the three sources of I_{Na} seen in Fig 5A) trains of at least 20 APs were used. **B.** Na^+ entry plotted to assess the cost/AP at different frequencies, as labeled and as explained in the text. Starred region beyond 600 Hz signifies that although this is beyond the species range, Epm is still able to produce regular APs at 650 Hz (though not, as seen in **B**, at 700 Hz). Calculations were done by requiring that V_{peak} = 12.86 mV for each frequency but this is referred to throughout the paper as 13 mV. Larger fonts for gNa_{max} values at 200 Hz and 600 Hz emphasize that these represent the extremes of the biological range for *Eigenmannia* EODs.

https://doi.org/10.1371/journal.pone.0196508.g006

Is all depolarizing Na^+-entry equivalent?

If synaptic stimuli with amplitudes different from $syn_{clamp}1$ are used, does this picture change? Fig 7 examines this question, with Fig 7A showing $V_m(t)$, plus the key attendant currents for a single AP triggered by pulsatile (200 Hz) $syn_{clamp}1$ or $syn_{clamp}5$ (a value 5 times larger than $syn_{clamp}1$). As expected, the AP rise time is faster with the stronger synaptic input, but the I_{Na} and I_K profiles are similar for both inputs. Fig 7B provides a comparison over this range of stimulus amplitudes. The black dashed-line shows that $syn_{clamp}1$ triggers APs of V_{peak} = 13 mV and that V_{peak} changes little with larger stimuli. And strikingly, the larger stimuli hardly alter the total Na^+-entry cost. Even though the increased stimulus ("more clamped-open AChRs") is allowing more Na^+-entry by this route (see the strong rise of the red line), total Na^+-entry (green line) into the electrocyte increases only slightly. With much more of the depolarization accomplished early due to Na^+ influx through AChR channels, the need for influx through Nav channels once they activate is diminished.

Would this outcome signify that a fish could be energetically "indifferent" to which class of channels carry the major load for depolarization? We suggest not. A cost analysis based solely on redressing Na^+-entry into electrocytes ignores metabolic costs incurred pre-synaptically. Costs related to producing and packaging AChR molecules is not captured by the Na^+-entry tally. Biologically, therefore, if EOs are driven by pulsatile synaptic stimuli, operating near our reference state (i.e. coordinates 1,1 of Fig 7B) would be optimal, ensuring signal integrity while avoiding high presynaptic costs.

Whereas Fig 7B deals only with APs at 200 Hz, Fig 7C looks also at 600 Hz. Both **Fig** 7B and 7C have dashed black lines for the 200Hz V_{peak}, but note that the Y-axis in Fig 7C is the absolute value of V_{peak}. Note too that for X-axis position "$syn_{clamp}1$" in Fig 7C, for each of the 3 plot lines, the relevant APs would be those from Fig 5B (top panels)**.**

The question here: to produce a full sized V_{peak}, could larger pulsatile stimuli (up to 10X $syn_{clamp}1$) compensate for an otherwise too-low gNa_{max}? The consequences of larger stimuli are qualitatively the same across the frequency range, as shown in Fig 7C which varies syn_{clamp} for 200 Hz and 600 Hz, with appropriate gNa_{max} values (see mauve and black dashed lines; the blue plot simply demonstrates that gNa_{max} appropriate to 200 Hz makes full amplitude APs at 600 Hz impossible for any stimulus intensity). Near $syn_{clamp}2$, AP peaks are slightly more depolarized than for $syn_{clamp}1$ and all-or-none behavior is particularly robust, with stimulus intensity variations of ~±0.3 in yield essentially the same AP amplitude. Rightward in the plots, V_{peak} values fall; larger syn_{clamp} becomes counterproductive.

Would the somewhat more robust all-or-none behavior near $syn_{clamp}2$ make it preferable to $syn_{clamp}1$? Not necessarily, since synaptic transmitter costs would nearly double. Taken together, Epm predicts (based on the three curves of Fig 7C) that across *Eigenmannias*'s 200–600 Hz EOD range, adequately large APs would be attained via appropriately-sized gNa_{max}, not by augmenting stimulatory AChR currents. Similarly, variations in gK_{max} cannot maintain V_{peak} across these frequencies. A Nav channel density adequate for the low end of the *Eigenmannia* EOD frequency

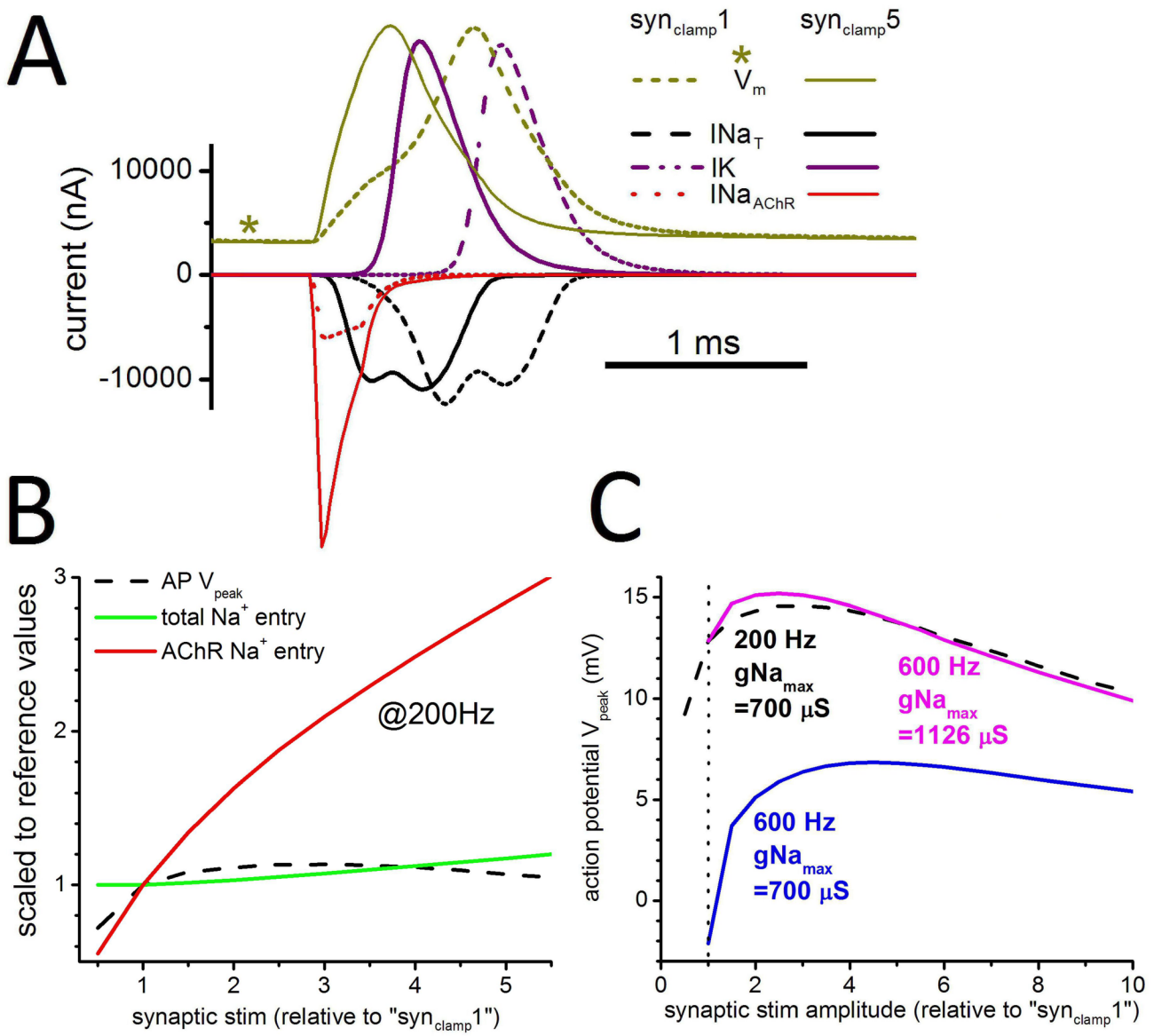

Fig 7. Effect of pulsatile stimulus amplitude. A. Single APs elicited by the standard pulsatile stimulus ($V_m(t)$ units are arbitrary, with the $syn_{clamp}1_{200Hz}$ AP as reference) calculated for $syn_{clamp}1_{200Hz}$ or $syn_{clamp}5_{200Hz}$, and V-gated currents (INa_T, where T signifies the transient component; persistent INa not shown), IK (delayed rectifier) plus the INa component of current through the AChR channels; gNa_{max} = 700 μS, stimuli at 200 Hz. **B.** For such APs elicited by pulsatile synaptic stimulation at increasing intensities (from $syn_{clamp}0.5_{200Hz}$ to $syn_{clamp}5.0_{200Hz}$), Na^+-entry via the stimulus (AChR) channels increases dramatically (red) but total Na^+-entry (green) is almost unaffected. The V_{peak} is relatively insensitive to stimulus intensity beyond syn_{clamp} = 1 (an "all-or-none" AP feature). **C.** Further testing of pulsatile syn_{clamp} intensity, for APs at 200 Hz and 600 Hz with the gNa_{max} values indicated. The dashed black line in **C** is equivalent to the dashed black line in **B** (where values are normalized).

https://doi.org/10.1371/journal.pone.0196508.g007

range could not be compensated for in high frequency fishes by adjusting gK_{max} (data not shown). This leads to the broad prediction that AChR density would be similar for fish operating at low and high frequencies, while Nav channel density would increase for higher frequency fish. With <2-fold difference in gNa_{max} predicted for 200 Hz vs 600 Hz fish, however, experimentally quantifying such moderate density differences may be challenging.

Simulating electrocyte action potentials during rapid changes in EOD frequency

In *Eigenmannia* and related electric fish, the close proximity of two fish with similar EOD frequencies produces beat frequencies that are detrimental to electrolocation [37–40]. Fish respond with a jamming avoidance response to increase beat frequency (i.e. increase their frequency differences), wherein the fish with the higher frequency increases its EOD frequency by ~5–10 Hz while the fish with the lower EOD frequency decreases its frequency by a similar magnitude. When fish increase EOD frequency during the JAR, how is the amplitude of the electrocyte AP maintained? To achieve higher AP frequencies for a JAR, *Eigenmannia* individuals could quickly augment the Nav channel density in their electrocytes' posterior membranes as proposed in earlier work [6]. Based on the Epm however, this costly procedure might be unnecessary. Within this model, extant excitability machinery could produce a typical JAR (i.e. 10 Hz above baseline frequency) with minimal loss of AP integrity. Fig 8 shows that in a fish with baseline EOD 400 Hz (with gNa_{max} = 783 μS), V_{peak} would change by only ~-0.25 mV during a +10Hz JAR., at 410 Hz, a ΔV_{peak} of ~-0.25 mV. This slightly diminished V_{peak} it

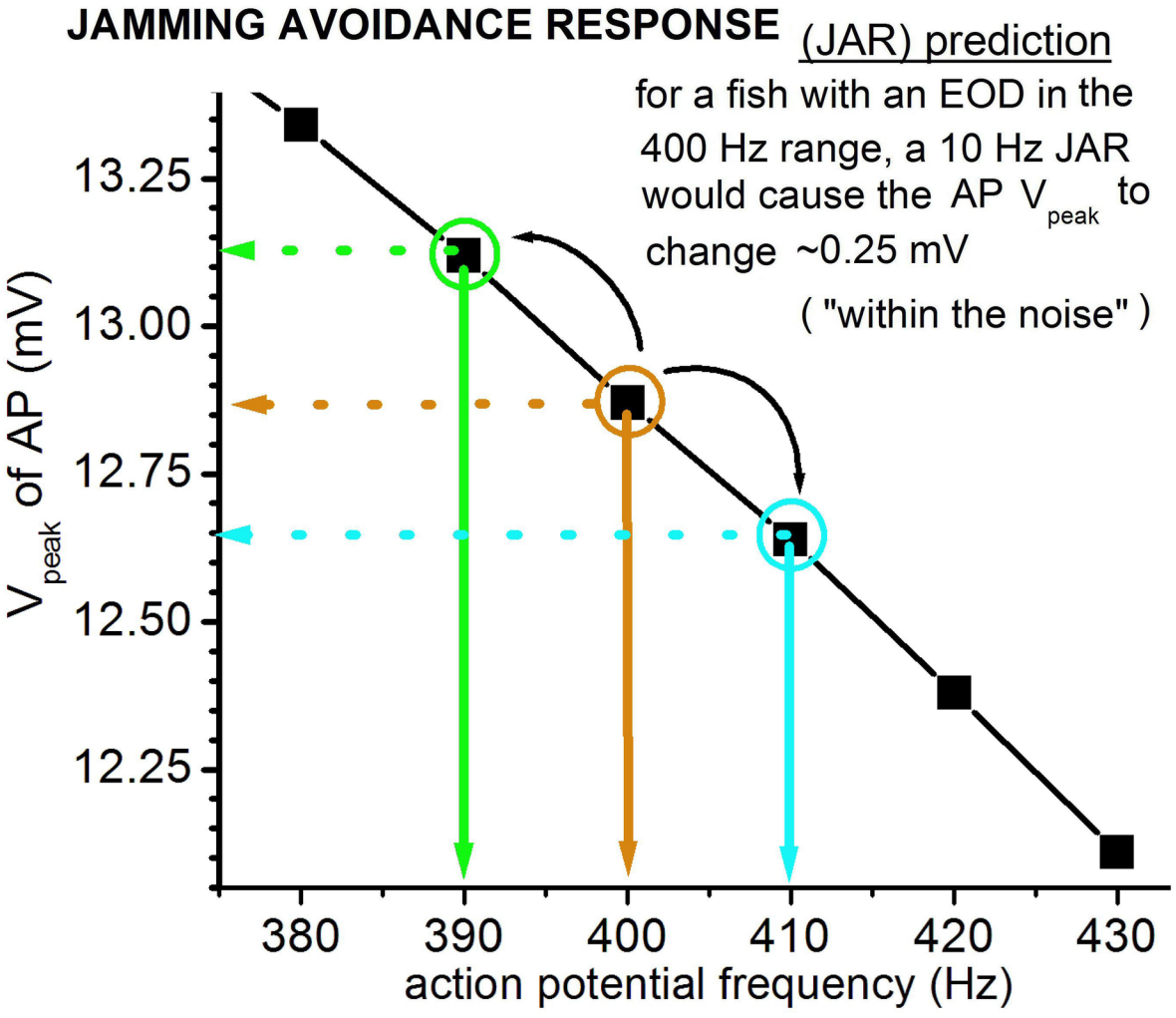

Fig 8. Simulation of a JAR. For APs at frequencies ± 10 Hz near 400 Hz, with gNa_{max} at 783 μS, V_{peak} differs minimally. This suggests that typical ± 10 Hz JARs in *Eigenmannia* might require no increased expression of Nav channels.

https://doi.org/10.1371/journal.pone.0196508.g008

should be noted, would be available with no time lag and would reverse immediately when the need for the JAR ended. The difference would be "within the noise" and thus would not be expected to jeopardize EOD signalling integrity.

If JARs occurred frequently, and if signal integrity needed to be even better than the ± 0.25 mV of Fig 8**,** then the issue of JAR dynamic range could be an important determinant of a fish's "choice" of (central nervous system-determined) stimulus-frequency, given its electrocyte $gNa_{max.}$ If a 400 Hz fish operated with a gNa_{max} somewhat greater than 783 μS, then its JAR plot (not shown) would be shallower than in Fig 8; likewise across the species frequency range.

Synaptic stimulation with a non-zero background

On timescales of many hours, *Eigenmannia* individuals rigorously maintain their particular EOD frequency. Thus far (**Figs** 5–7), the background [ACh] in the synaptic cleft ("$[ACh]_{synaptic}$") is assumed to decay rapidly toward zero after each invariant pulsatile stimulus. But instead, could maintenance of $[ACh]_{synaptic}$ be responsible for setting an invariant frequency? Here we briefly consider this other extreme, plus the more likely situation in which reliably large pulsatile Δ $[ACh]_{synaptic}$ stimuli ride atop a non-zero background $[ACh]_{synaptic}$.

Fig 9Ai shows Epm APs for various constant or steady-state levels of AChR activation (i.e., 0 Hz stimulation) for gNa_{max} = 700 μS. Fig 9Aii shows that a threshold for AP generation occurs at ~$syn_{clamp}0.0092_{0Hz}$ (initial point in the plot). As $syn_{clamp0Hz}$ increases above this threshold, the AP frequency rises from 0 Hz until at $syn_{clamp}0.05_{0Hz}$ APs (with V_{peak} = 9.0 mV) fire at ~200 Hz, the bottom of the species' EOD range. With increasing $syn_{clamp0Hz}$ intensity (as with increasing I_{clamp} intensity, see **Figs** 5 and 6) the AP frequency increases but V_{peak} falls (see $syn_{clamp}0.40_{0Hz}$ in Fig 8Ai) unless, as shown in Fig 9Aiii, gNa_{max} is made larger. This shows that, in principle, APs at frequencies required to drive EODs up to 600 Hz could be elicited using a constant-amplitude AChR conductance. In practice, inherent sources of noisy Δ $[ACh]_{synaptic}$ (e.g. as in *Torpedo* electroplax recordings by Giirod et al [24]) would make the EOD frequency unacceptably variable.

In Fig 9B APs are stimulated by an imposed $\Delta[ACh]_{synaptic}$ that combines pulsatile and background syn_{clamp} (the 0 Hz level was set at 80% of threshold, i.e., $syn_{clamp}0.0074_{0Hz}$). Fig 9Bi shows $V_m(t)$ when either $syn_{clamp}0.1_{200Hz}$ (orange) or $syn_{clamp}0.4_{200Hz}$ (blue) are added atop this 0 Hz background. The former (orange) is insufficient to achieve the target AP frequency (200 Hz) whereas the latter (blue) is sufficient. Over 4 cycles, the $syn_{clamp}0.1_{200Hz}$ stimuli summate to trigger 50 Hz APs. When the membrane depolarizes due to Na^+ entry from pulsed cholinergic stimuli, both transient and persistent gNa changes contribute to maintaining the voltage gain between pulses because in that voltage range inactivation is inconsequential ($h \approx 1$). With a fixed subthreshold background ($syn_{clamp}0.0074_{0Hz}$) a plot of AP frequency versus 200 Hz stimuli of increasing amplitude generates a "devil's staircase" plot [41] Fig 9Bii). Below the critical pulsatile stimulus amplitude required for any given AP frequency, it would be possible, given a noise-free system, to discern period doubling, tripling etc. In the case illustrated here (i.e., 200 Hz APs) $syn_{clamp}0.32_{200Hz}$ is the relevant critical stimulus, and because the modeling is noise-free, period doubling and tripling is evident (plateaus are evident at 100 Hz and 66.6 Hz, i.e. one-half and one-third of the stimulation frequency, 200Hz) in Fig 9Bii. For real systems, given the temporal stochasticity of ACh release and the inherent variation in quantal size at the time of release, variations in both pulsatile and background stimulus amplitudes would be expected. This would increase the critical pulsatile stimulus amplitude required for reliable firing at the target frequency; that amplitude would more likely be reached further along the top of the staircase (e.g. at one of the grey arrowheads) than in a noise-free simulation.

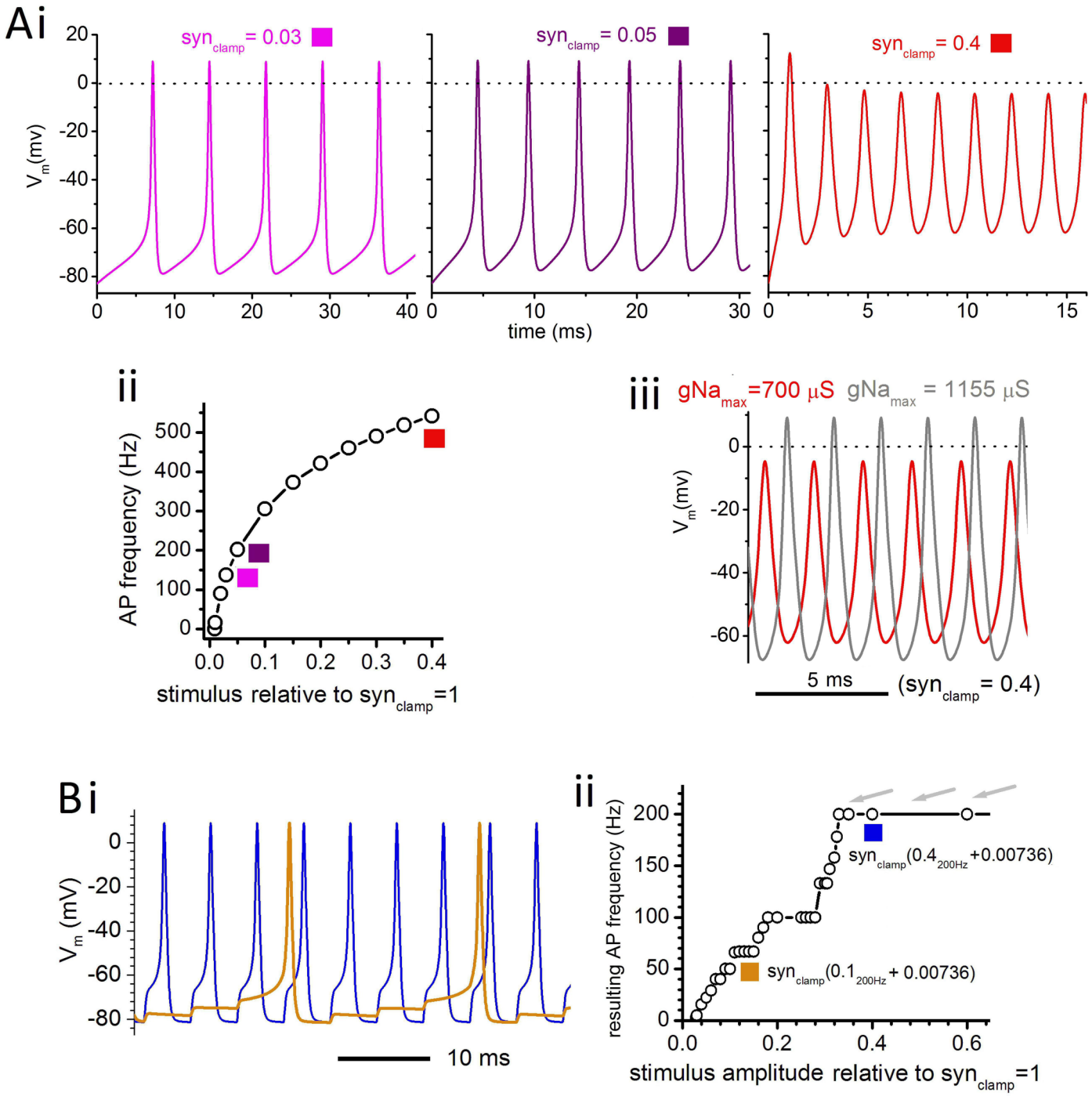

Fig 9. Background synaptic stimulation. Ai. Epm APs for three steady-state (i.e. 0 Hz) levels of AChR activation, $syn_{clamp}0.03_{0Hz}$, $syn_{clamp}0.05_{0Hz}$, and $syn_{clamp}0.4_{0Hz}$ fire at 137 Hz, 202 Hz, and 541 Hz respectively (gNa_{max} = 700 μS throughout). **Aii.** Epm AP frequency as a function of stimulus intensity (conditions as in **Ai**); squares color-coded for the plots in **Ai**. **Aiii.** Red trace at 541 Hz firing (conditions as in **Ai**) with a second overlaid trace showing APs when gNa_{max} is increased to 1155 μS (this produces APs of V_{peak} = 9 mV, i.e., the same as for $syn_{clamp}0.03_{0Hz}$ with gNa_{max} = 700 μS). **Bi.** APs elicited by a 200 Hz pulsatile stimulus in the presence of a subthreshold background stimulus ($syn_{clamp}0.00736_{0Hz}$). For $syn_{clamp}0.1_{200Hz}$ (orange) the output AP frequency is 50 Hz whereas for $syn_{clamp}0.4_{200Hz}$ (blue) the target frequency of 200 Hz is attained. **Bii.** This background stimulus ($syn_{clamp}0.00736_{0Hz}$) plus 200 Hz pulsatile stimuli at the amplitudes indicated elicits APs at different frequencies as shown here in a "devil's staircase" plot.

https://doi.org/10.1371/journal.pone.0196508.g009

Na^+ entry for different stimulus regimes

We further wondered how different combinations of background and pulsatile synaptic stimulation would affect Na^+ entry at frequencies spanning 200 to 600 Hz, the species EOD range (we consider APs of a fixed value, V_{peak} = 13 mV; gNa_{max} was adjusted accordingly). Lewis et al. [6] determined EOD-linked O_2 consumptions at the whole animal level, not at the level of electrocytes. Here, we stress that from the perspective of whole animal energetics, a Na^+ ion entering an electrocyte through a Nav channel (gNa) versus a Na^+ ion entering an electrocyte through an AChR almost certainly presents a different (whole animal level) cost. Given an appropriate Na^+ gradient, a Nav channel simply has to open in response to depolarization to allow Na^+ to enter, but for Na^+ entry via an AChR channel, ACh must first be manufactured and packaged and delivered (at a cost) then released via presynaptic depolarization (at a cost). Accordingly, both total and pathway-specific Na^+ entry into the electrocyte was tallied. Table 2 lists outcomes for APs firing at 200 Hz, 500 Hz and 600 Hz. The frequency 500 Hz was included to show how Na^+ entry/AP evolves as the system approaches its upper limit.

The stimulus extremes, i.e. purely pulsatile and purely steady-state (0 Hz) stimulation are represented by rows **1**, **7**, **13** and rows **6**, **12**, **18** respectively. The former reiterates Fig 6B, i.e., synaptic components essentially constant across frequencies while Na^+ entry/AP through Nav channels increases nonlinearly with frequency. For the latter (rows **6**, **12**, **18**), total Na^+ entry for 0 Hz syn_{clamp} is considerably higher than for pure pulsatile, most markedly so at the high frequency end. Taken together with the argument that 0 Hz syn_{clamp} in vivo would not on its own generate reliable clock-like EODs, it is difficult to conceive of any benefit of a pure 0 Hz regime.

For AP target frequencies 200 Hz, 500 Hz, 600 Hz, the intermediate rows explore situations with some level of $[ACh]_{synaptic}$ persisting between pulsatile stimuli, i.e., combinations of $syn_{clamp0Hz}$ >0 plus a pulsatile syn_{clamp} at some level. For each target frequency, two values of $syn_{clamp0Hz}$ were tested, one subthreshold, the other strongly suprathreshold. Subthreshold was represented by 80% of the 0 Hz threshold (rows **2**, **3**, **8**, **9**, and **14**, **15**), and suprathreshold was represented by the 0 Hz syn_{clamp} amplitude that elicits firing at ~70% of the target frequency (rows **4**, **5**, **10**, **11**, and **15**, **16**). In Table 2, footnotes list how, as target frequency increases, the $syn_{clamp0Hz}$ threshold decreases (this occurs because the gNa_{max} imposed to maintain V_{peak} = 13 mV yields a more excitable system).

To provide a basis of comparison in the intermediate (mixed stimuli) rows, each of the two chosen 0 Hz syn_{clamp} amplitudes is first tested in conjunction with the "control" pulsatile amplitude (first column of rows **1**, **7**, **13**) needed for 13 mV AP trains at the target frequency (i.e. rows **2**, **8**, **14**), albeit with gNa_{max} slightly reduced (to maintain V_{peak} = 13 mV). Next (rows **3**, **9**, **15**), with the same subthreshold background, a pulsatile amplitude was found that slightly exceeds the minimum needed to achieve the target AP frequency. For 200 Hz for example, this is slightly rightward of the left margin of the "devil staircase"plateau (Fig 9Bii; $syn_{clamp}0.34_{200Hz}$ was used here, row **3**). For the "0 Hz suprathreshold-to-70%-target" cases, the Na^+-entry results are in rows **4** and **5** for 200 Hz, **10** and 11 for 500 Hz, and **16** and **17** for 600 Hz. Thus, across all frequencies, total Na^+-entry is minimal if there is no steady-state component to the stimulus (rows **1**, **7**, **13**) but if this is not achievable, then the most cost-effective approach appears to be maintaining background synaptic stimulation as low as possible.

The question of which combination of depolarizing Na^+ entry is most economical will depend on how much more expensive synaptic Na^+ entry is compared to Nav Na^+ entry. For example, if Na^+-entry through AChRs incurred 10X the whole-body metabolic cost of Na^+ entry through Nav channels, then regimes that reduced entry through AChRs (e.g., rows **3**, **5**, **6** for 200 Hz) would be beneficial. There, the reduced pulsatile component yields a marked

Table 2. Na^+ entry for various synaptic stimulus regimes$^{\Delta}$.

row #	syn_{clamp} (amplitudes)		$gNa_{max}{}^{\Delta}$(μS)	Na^+ entry/AP ($x10^9$)		
	0 Hz part (thr 0.0092) *	**200 Hz part**		**Total entry** (Nav+AChR)	**Nav**	**AChR**
1	0	1	700	59.2	48.7	10.5
2	0.0074	1	698	59.6	48.2	11.4
3	0.0074	0.34	835	66.8	61.6	5.2
4	0.03 (→ 137 Hz)	1	714	62.2	48.4	13.8
5	0.03	0.16	824	66.8	60.2	6.6
6	0.048*	0	819	67.1	59.6	7.5
	0 Hz part (thr 0.0080)**	**500 Hzpart**		**Total entry** (Nav+AChR)	**Nav**	**AChR**
7	0	1	897	70.1	59.8	10.3
8	0.0064	1	896	70.2	59.7	10.5
9	0.0064	0.68	1015	76.2	68.4	7.8
10	0.12 (→ 345 Hz)	1	925	74.9	59.6	15.3
11	0.12	0.45	1008	78.2	67.1	11.1
12	0.28**	0	1097	85.7	71.2	14.5
	0 Hz part (thr 0.0067) ***	**600 Hzpart**		**Total entry** (Nav+AChR)	**Nav**	**AChR**
13	0	1	1126	88.3	77.3	11.0
14	0.0054	1	1124	88.3	77.1	11.2
15	0.0054	0.85	1238	93.8	83.9	9.9
16	0.18 (→ 414 Hz)	1.0	1170	94.4	76.9	17.5
17	0.18	0.7	1219	96.2	80.9	15.3
18	0.47***	0	1569	126.0	103.0	23.0

Syn_{clamp} amplitude is non-dimensional (as explained in the section entitled "**Epm responses to pulsatile synaptic current stimulation**"), gNa_{max} is in μS and Na^+ entry/AP is as defined for Fig 6B.

As explained in the text, the 0 Hz background (or subthreshold level) for any set of conditions was chosen to be 80% of threshold for those conditions. Using 75% and 85% of threshold instead yields AP peak amplitudes identical to those for 80% to within 0.01 mV and Na^+ entry values identical to within 0.2%.

$^{\Delta}$ for each stimulus regime gNa_{max} is adjusted until V_{peak} = 13 mV (hence the threshold values given below vary with frequency)

* $syn_{clamp}0.0092_{0Hz}$ brings this system to firing **thr**eshold

$syn_{clamp}0.048_{0Hz}$ causes this system to fire at 200 Hz

** $syn_{clamp}0.0080_{0Hz}$ brings this system to firing **thr**eshold

$syn_{clamp}0.28_{0Hz}$ causes this system to fire at 500 Hz

*** $syn_{clamp}0.0067_{0Hz}$ brings this system to firing **thr**eshold

$syn_{clamp}0.47_{0Hz}$ causes this system to fire at 600 Hz

https://doi.org/10.1371/journal.pone.0196508.t002

saving in pulsatile ACh, though at higher frequency (rows **9**, **15**) the relative benefit diminishes. As Table 2 shows, the pulsatile syn_{clamp} component required to override the natural firing frequency of the purely fixed amplitude stimulation is larger than for the subthreshold background, and increases with frequency. Nevertheless, at 500 Hz, if the AChR entry pathway was 10X more expensive (as per our suggestion here) then, for rows **10** and **11**, row **11** might be less expensive at the whole-animal level, even though row **10** shows the smaller total Na^+-

entry. In other words, if clearing the synapse of ACh between pulses was not possible, then minimizing the pulsatile amplitude would be beneficial.

Overall, the results of Table 2 provide some important insights. Between stimulatory pulses (especially at higher frequencies), if electrocyte synapses could not fully remove ACh, an energy efficient system would need to optimize the ratio of background-to-pulsatile amplitude to minimize Na^+ entry through AChRs. There is no penalty for background ACh provided it is subthreshold. In fact, at low frequency, there is even a saving from a subthreshold background provided the pulsatile component is reduced. Even with a suprathreshold background, the system can fire at reasonable cost, but with costs rising more steeply with frequency than in the case of a purely pulsatile stimulus or with a combined pulsatile and subthreshold background. Even with the caveat that the entry pathway specific differential is as yet unknown, Table 2 suggests that a moderate background ACh is not detrimental, but that fish generating EODs at the higher end of the frequency range would have relatively little latitude for lowering synaptic costs by increasing the background.

Calculated electrocyte costs versus whole-animal measurements

Lewis et al. [6] provided whole animal O_2 consumption data for nine fish generating EODs at frequencies $>$ 300 Hz and $<$ 500 Hz. The data were fit to an exponential. With Epm, we calculated electrocyte Na^+ entry at frequencies from 200 Hz to 600 Hz. At 200 Hz and below, all Epm parameters return to their pre-stimulus values prior to the next stimulus (in other words, from 0 to 200 Hz, a plot for ATP/AP(Hz) is a flat line. Above that, the values rise non-linearly, though not exponentially. We nevertheless fit an exponential to our Epm-calculated points (for entry through both Nav and AChR channels) at 300, 400 and 500 Hz, and that exponential predicts a 1.17-fold increase between 300 and 500 Hz whereas the Lewis et al. [6] fit over that same range gives a 6.05-fold increase. With Na+ entry/AP through the AChR channels essentially constant across all frequencies (Fig 6), the small but distinct increase with frequency is attributable to influx into the electrocyte through the increasing numbers of Nav channels. However, while Nav channel activation depends only on the voltage of membranes in which the channels are embedded, AChR channel activation depends on a plethora of "upstream" processes whose costs would contribute to whole-animal O2 consumption, but not to the cost of electrocyte ion homeostasis. Therefore, the very large frequency dependent discrepancy (slopes of 6.05 vs 1.17) indicates that the very high cost of EODs at the high end of *Eigenmannia*'s frequency range cannot reasonably be attributed to electrocyte excitability. Instead it suggests that neural events preceding the electrocyte-based APs, along with costs of circulatory processes that help ensure that electrocytes maintain ion homeostasis are substantially responsible. Perhaps this helps explain why the very high frequency *Apteronotid* species have a 'neurogenic' electric organ in which neurally-derived electrocytes receive direct electrotonic inputs without a chemical synapse[42].

Discussion

Electrocyte action potentials (APs) underlie the wave-type electric organ discharge (EOD) of *Eigenmannia*. This continuous high frequency bioelectrical phenomenon is sustained over the lifespan of the fish. An explanation for how *Eigenmannia* unerringly maintains its EOD requires a better understanding of how the electrocytes produce APs at 200–600 Hz, of the metabolic demands this incurs, and of how subcellular, cellular and tissue geometry along with the associated molecular components are organized to meet these demands [6, 42]. In addition, this knowledge should yield insights for energetic strategies in other highly active excitable tissues including brain and skeletal muscle [17]. Assessing the contribution of electrocyte

APs to the whole-animal metabolic cost measured by Lewis et al. [6] requires a thorough accounting of the ionic and biophysical mechanisms of electrocyte APs and post-synaptic currents. Electrophysiology has revealed some of the ionic conductances contributing to electrocyte firing [6, 16], and cyto-histochemistry is showing the locations of ion channels and pumps in the large and highly polarized electrocytes [5]. Here, a computational model for the excitable innervated posterior region of electrocyte membrane is updated to better reflect functional characteristics of electrocytes and to better depict molecular mechanisms of electrocyte excitability.

In the new model, Epm, addresses some limitations inherent in a previous computational model for *Eigenmannia* electrocyte APs. As done previously [16], however, we assumed here that across all EOD frequencies, APs attain the same peak depolarization (V_{peak}) and voltage-gated channel kinetics are constant. Again, as previously, the model includes a delayed rectifier conductance (see Methods) even though one has not yet been found in *Eigenmannia* electrocytes. For Epm, we arbitrarily retained the same (frequency-invariant) gK_{max} as previously, then tuned the Hodgkin-Huxley type kinetic parameters for gK(V) and gNa(V) to ensure that sustained APs were possible at 600 Hz, as per the Methods. A major change in the present model of the electrocyte's innervated posterior membrane is the inclusion of a biophysically appropriate post-synaptic cation conductance. Note that until these specific assumptions are tested, these models are predictive and as a "proof of principle".

Importantly, adjusting only one parameter in Epm enables the production of APs with consistent amplitude at frequencies up to 600 Hz, the upper end of the species' EOD frequency range. This parameter is gNa_{max} and corresponds to Nav channel density. Epm exhibits more robust excitability than previous models; it produces all-or-none APs that start from a lower firing threshold, and it fires repetitively with moderate levels of constant current stimulation. It predicts, moreover, contrary to previous models, that electrocytes could achieve a transient jamming avoidance response (this entails a change in discharge frequency of approximately 10 Hz) with no requirement to alter channel properties or channel densities.

The updated model leads to two key predictions and questions for further experimental and computational work. Firstly, a strong prediction from Epm (gleaned from analysis of the distinct Na^+-entry budgets for Nav and AChR channels and from exploring the costs of varying the densities of both types of channels) is that electrocyte Nav channel density should increase non-linearly with increasing EOD frequency, whereas AChR channel density is expected to be constant with frequency. Secondly, the analysis here indicates that the electrocyte AP itself is a relatively energy-efficient process and is not the major contributor to the whole-animal metabolic cost of EOD production. Instead, the Epm analysis predicts that a much greater proportion of the whole-animal costs associated with EOD production would arise from events "upstream" of the post-synaptic and AP currents. These upstream processes would be those necessary to bring about high frequency activation of the electocytes' post-synaptic AChRs. Included here would be the continual presynaptic manufacture and vesicular packaging of ACh molecules as well as the costs associated with producing high frequency electromotor neuron and central neuronal pacemaker action potentials [42]. Insofar as the electrocyte's extensive capillary beds contribute to maintenance of extracellular Na^+ and K^+ levels, part of the metabolic costs of continually producing high frequency EOD will also be associated with remote sites such as kidney and gills where circulatory levels of these ions are regulated.

Thus, while Epm applies only to the posterior excitable membrane and assumes that dissipation of E_{Na} occurs only across that membrane, this should not be taken to mean that homeostatic mechanisms that maintain posterior membrane E_{Na} and E_K occur exclusively at the posterior membrane. What it implies is that the overall complex (electrocyte/electric organ/

circulatory system) is able to regulate the posterior membrane E_{Na} and E_K values within very narrow bounds. An important part of the system that has yet to be explored is the posterior and anterior regions' K-selective inward rectifier channels and the extensive fine t-tubule-like invaginations (given the evolution of electrocytes from skeletal muscle; [32, 43, 44]. Whereas dissipation of electrocyte E_{Na} is a posterior membrane process, dissipation of electrocyte E_K is surely an electrocyte-wide process. Ongoing efforts are devoted to developing a full model of the *Eigenmannia* electrocyte that incorporates whole-cell ion homeostasis and the simultaneously occurring processes at both anterior and posterior membranes.

As indicated earlier, Epm includes a necessary "place holder" conductance (the gK(V)) whose physiological role is to achieve fast repolarization of the AP. Ongoing experimental work seeks the molecular identity of this necessary entity. One possibility is an as-yet unidentified K_{Na} channel with rapid voltage dependent kinetics and/or extremely high Na^+ sensitivity. Another possibility is a fast voltage-gated Cl^- channel.

It is self-evident that continual high frequency electrocyte firing with near-zero variance requires near-perfect ion homeostasis and accordingly Epm assumes invariant E_{Na} and E_K. In principle, the *sine qua non* for perfect ion homeostasis is perfect reciprocal-transport: for each Na^+ ion that enters, one Na^+ ion is pumped out. Thus even with no explicit $3Na^+/2K^+$-ATPase "sodium pump" the model predicts excitability-imposed ATP requirements (and by extension, the required O_2 consumption) by tallying all excitability-related Na^+-entry. We again stress, however, that what is not self-evident, is the question of where (i.e., across which membranes and with what geometry) $3Na^+/2K^+$ pump activity would be best deployed to maintain invariant E_{Na} and E_K at the posterior membrane. E_K or E_{Na} dysregulation can readily produce pathological patterns of excitability [18] yet astonishingly little is known about the role of cyto-geometry in the Na^+/K^+ homeostatic "near-perfection" of high-frequency excitable systems. Epm is therefore a step towards a longer term goal of learning precisely where *Eigenmannia* spends ATP to sustain EODs. Since the $3Na^+/2K^+$-ATPase is electrogenic, if homeostatic pumping occurred entirely across the same membrane site that generates the high-frequency APs, the dissipative process (ion channel currents) would have to perfectly balance every 3 incoming Na^+ with 2 outgoing K^+. Any departure from this pump-imposed constraint would lead to membrane polarization and thus jeopardize the precision of high frequency AP production. If instead, the work of ion homeostasis is partly off-loaded to non-excitable electrocyte regions (e.g., anterior membrane, tubular invaginations of the posterior membrane) and/or to remote organs such as kidney, there would be latitude for diverse flux machinery to offset pump induced polarization (e.g. cation leak channels, inward rectifiers, sodium-activated gK, etc) without jeopardizing the posterior membrane APs. With Epm therefore, we set explicit homeostatic pumping aside to make it possible to quantify (via posterior membrane Na^+ entry) what the electrocyte achieves as it maintains perfect homeostasis.

Reardon et al [45], examined EOD frequency and amplitude in *Eigenmannia* under reduced water oxygenation. In these experiments hypoxia did not alter EOD frequency, but extreme hypoxia is associated with decreased EOD amplitudes (independent of EOD frequency). This suggests that under these experimental conditions the metabolic cost of EOD signalling may not increase with frequency as dramatically as was observed in later work [6]. This is in line with our present results on AP-related Na+ costs. Note however that Lewis et al measured the direct cost of changing EOD frequency during a jamming responses while EOD amplitude was maintained. So alternatively, EOD frequency could be more vigorously protected (than EOD amplitude) under environmental challenges like hypoxia.

Voltage-clamp data from electrocytes of the lower frequency gymnotid, *Sternopygus*, led to the intriguing suggestion that Nav and Kv channel kinetics are jointly modulated along a continuum such that lower frequency EODs arise from slower channels and higher frequency

EODs from faster channels [46, 47]. No confirmatory current clamp data showing AP shapes were obtained, but the idea is to generate at all frequencies, appropriate-shaped APs for yielding sinusoidal EODs. We did not test this as a feature in Epm because, in conjunction with an appropriate pacemaker output, it implies the existence of extraordinarily complex (and perhaps biologically implausible) co-regulation of the kinetics of two discrete channel protein complexes. In any event, use of an invariant set of kinetic parameters in Epm yielded APs whose shape differed little between 200 Hz and 600 Hz. For electrocytes from fish of known EOD frequency, it would be instructive to measure V_m while driving the input neuron at different frequencies and to perform current clamp experiments as suggested in **Fig 3**.

Conclusion

The two core questions driving the current study are broadly applicable to excitable cells in general: 1) what mechanisms enable sustained high-frequency firing? and, 2) what are the relative contributions of membrane excitability, synaptic processes, and organismal-level processes to the metabolic costs of high-frequency firing? The electric organ discharge of *Eigenmannia* is a powerful and accessible system where experimental work on the physiology of EOD production and computational modeling of these physiological processes can form a synergistic and mutually informative approach to answering these questions. An intriguing example of the potentially broad cell physiological relevance of *Eigenmannia* comes to light in the neural processing of high frequency auditory signals [48]. Energetics issues faced by *Eigenmannia* electrocytes arise also for auditory neurons, but to our knowledge how pumps are deployed to ensure post-synaptic homeostasis at high frequency auditory synapses is unknown. Transmission electron microscopy of both *Eigenmannia* electrocytes and auditory synapses reveal abundant but unexplained post-synaptic membrane "vesicles" of unknown function and topology. Perhaps these vesicles are tortuous invaginations that could contribute to ion homeostasis as noted above. For *Eigenmannia*, we showed that this region stains intensely for Na^+/K^+ pumps [5] and in skeletal muscle, pumps are an important component of t-tubular membrane. Pursuing the role of these membranous structures in *Eigenmannia* electric organ energetics could, we suspect, shed light on the cellular energetics of high frequency firing in the auditory system.

And looking beyond cell physiology/cell biology, a complete account of the mechanisms and energetics of high frequency firing will have far-reaching implications for understanding processes as varied as the evolution of nervous systems [49, 50], tradeoffs in sensorimotor systems [51] and neuroecological adaptations in animal behavior [52].

Acknowledgments

B.J. and J.E.L. acknowledge support from the Natural Sciences and Engineering Research Council (Canada) and C.E.M. from the Ottawa Hospital Research Institute. M.R.M. acknowledges support from the National Science Foundation grants IOS1257580 and IOS1350753.

Author Contributions

Conceptualization: Bela Joos, Catherine E. Morris.

Formal analysis: Bela Joos, Catherine E. Morris.

Funding acquisition: Bela Joos.

Methodology: Bela Joos, Catherine E. Morris.

Software: Bela Joos.

Validation: Bela Joos, Michael R. Markham, John E. Lewis, Catherine E. Morris.

Visualization: Bela Joos, Catherine E. Morris.

Writing – original draft: Bela Joos, Catherine E. Morris.

Writing – review & editing: Bela Joos, Michael R. Markham, John E. Lewis, Catherine E. Morris.

References

1. Attwell D, Laughlin SB. An energy budget for signaling in the grey matter of the brain. J Cereb Blood Flow Metab. 2001; 21(10):1133–45. Epub 2001/10/13. https://doi.org/10.1097/00004647-200110000-00001 PMID: 11598490.
2. Harris JJ, Attwell D. The energetics of CNS white matter. J Neurosci. 2012; 32(1):356–71. Epub 2012/01/06. https://doi.org/10.1523/JNEUROSCI.3430-11.2012 PMID: 22219296; PubMed Central PMCID: PMCPmc3272449.
3. Harris JJ, Jolivet R, Attwell D. Synaptic energy use and supply. Neuron. 2012; 75(5):762–77. https://doi.org/10.1016/j.neuron.2012.08.019 PMID: 22958818.
4. Lennie P. The cost of cortical computation. Curr Biol. 2003; 13(6):493–7. PMID: 12646132.
5. Ban Y, Smith BE, Markham MR. A highly polarized excitable cell separates sodium channels from sodium-activated potassium channels by more than a millimeter. J Neurophysiol. 2015; 114(1):520–30. https://doi.org/10.1152/jn.00475.2014 PMID: 25925327
6. Lewis JE, Gilmour KM, Moorhead MJ, Perry SF, Markham MR. Action potential energetics at the organismal level reveal a trade-off in efficiency at high firing rates. J Neurosci. 2014; 34(1):197–201. https://doi.org/10.1523/JNEUROSCI.3180-13.2014 PMID: 24381281
7. Logothetis NK, Wandell BA. Interpreting the BOLD signal. Annu Rev Physiol. 2004; 66:735–69. Epub 2004/02/24. https://doi.org/10.1146/annurev.physiol.66.082602.092845 PMID: 14977420.
8. Murta T, Leite M, Carmichael DW, Figueiredo P, Lemieux L. Electrophysiological correlates of the BOLD signal for EEG-informed fMRI. Hum Brain Mapp. 2015; 36(1):391–414. Epub 2014/10/04. https://doi.org/10.1002/hbm.22623 PMID: 25277370; PubMed Central PMCID: PMCPMC4280889.
9. Eklund A, Nichols TE, Knutsson H. Cluster failure: Why fMRI inferences for spatial extent have inflated false-positive rates. Proc Natl Acad Sci U S A. 2016; 113(28):7900–5. https://doi.org/10.1073/pnas.1602413113 PMID: 27357684; PubMed Central PMCID: PMCPMC4948312.
10. Olfert IM, Baum O, Hellsten Y, Egginton S. Advances and challenges in skeletal muscle angiogenesis. Am J Physiol Heart Circ Physiol. 2016; 310(3):H326–36. https://doi.org/10.1152/ajpheart.00635.2015 PMID: 26608338; PubMed Central PMCID: PMCPMC4796623.
11. Schwartz IR, Pappas GD, Bennett MVL. The fine structure of electrocytes in weakly electric teleosts. J Neurocytol. 1975; 4(1):87–114. PMID: 1113145
12. Assad C, Rasnow B, Stoddard PK. Electric organ discharges and electric images during electrolocation. J Exp Biol. 1999; 202(Pt 10):1185–93. PMID: 10210660.
13. Assad C, Rasnow B, Stoddard PK, Bower JM. The electric organ discharges of the gymnotiform fishes: II. Eigenmannia. J Comp Physiol A. 1998; 183(4):419–32. Epub 1998/11/11. PMID: 9809452.
14. Markham MR. Electrocyte physiology: 50 years later. The Journal of Experimental Biology. 2013; 216(13):2451–8. https://doi.org/10.1242/jeb.082628 PMID: 23761470
15. Howarth C, Gleeson P, Attwell D. Updated energy budgets for neural computation in the neocortex and cerebellum. J Cereb Blood Flow Metab. 2012; 32(7):1222–32. Epub 2012/03/22. https://doi.org/10.1038/jcbfm.2012.35 PMID: 22434069; PubMed Central PMCID: PMC3390818.
16. Markham MR, Kaczmarek LK, Zakon HH. A sodium-activated potassium channel supports high-frequency firing and reduces energetic costs during rapid modulations of action potential amplitude. J Neurophysiol. 2013; 109(7):1713–23. https://doi.org/10.1152/jn.00875.2012 PMID: 23324315
17. Niven JE. Neuronal energy consumption: biophysics, efficiency and evolution. Curr Opin Neurobiol. 2016; 41:129–35. doi: dx.doi.org/10.1016/j.conb.2016.09.004. https://doi.org/10.1016/j.conb.2016.09.004 PMID: 27664945
18. Boucher PA, Joos B, Morris CE. Coupled left-shift of Nav channels: modeling the Na(+)-loading and dysfunctional excitability of damaged axons. J Comput Neurosci. 2012; 33(2):301–19. https://doi.org/10.1007/s10827-012-0387-7 PMID: 22476614.
19. Bennett MVL. Modes of operation of electric organs. Ann N Y Acad Sci. 1961; 94:458–509. PubMed Central PMCID: PMC0005.

20. Ferrari MB, Zakon HH. Conductances contributing to the action potential of *Sternopygus* electrocytes. Journal of Comparative Physiology A: Neuroethology, Sensory, Neural, and Behavioral Physiology. 1993; 173(3):281–92. PubMed Central PMCID: PMC0008.

21. Lester HA. Analysis of sodium and potassium redistribution during sustained permeability increases at the innervated face of Electrophorus electroplaques. J Gen Physiol. 1978; 72(6):847–62. PMID: 731201; PubMed Central PMCID: PMCPMC2228490.

22. Catania KC. The shocking predatory strike of the electric eel. Science. 2014; 346(6214):1231–4. https://doi.org/10.1126/science.1260807 PMID: 25477462.

23. Scheich H. Neural basis of communication in the high frequency electric fish,*Eigenmannia virescens* (Jamming Avoidance Response). Journal of Comparative Physiology A: Neuroethology, Sensory, Neural, and Behavioral Physiology. 1977; 113(2):181–206.

24. Girod R, Correges P, Jacquet J, Dunant Y. Space and time characteristics of transmitter release at the nerve-electroplaque junction of Torpedo. J Physiol. 1993; 471:129–57. PMID: 8120801; PubMed Central PMCID: PMCPMC1143955.

25. Stiles JR, Van Helden D, Bartol TM Jr., Salpeter EE, Salpeter MM. Miniature endplate current rise times less than 100 microseconds from improved dual recordings can be modeled with passive acetylcholine diffusion from a synaptic vesicle. Proc Natl Acad Sci U S A. 1996; 93(12):5747–52. PMID: 8650164; PubMed Central PMCID: PMCPMC39132.

26. Hodgkin AL, Huxley AF. A quantitative description of membrane current and its application to conduction and excitation in nerve. J Physiol. 1952; 117(4):500–44. PMID: 12991237; PubMed Central PMCID: PMC1392413.

27. Sterratt D. Principles of computational modelling in neuroscience. Cambridge; New York: Cambridge University Press; 2011. xi, 390 p. p.

28. Cannon SC, Brown RH Jr., Corey DP. Theoretical reconstruction of myotonia and paralysis caused by incomplete inactivation of sodium channels. Biophys J. 1993; 65(1):270–88. https://doi.org/10.1016/S0006-3495(93)81045-2 PMID: 8396455; PubMed Central PMCID: PMCPMC1225722.

29. Pappone PA. Voltage-clamp experiments in normal and denervated mammalian skeletal muscle fibres. J Physiol. 1980; 306:377–410. PMID: 6257898; PubMed Central PMCID: PMCPMC1283012.

30. Shenkel S, Sigworth FJ. Patch recordings from the electrocytes of *Electrophorus electricus*. Na currents and PNa/PK variability. J Gen Physiol. 1991; 97(5):1013–41. https://doi.org/10.1085/jgp.97.5.1013 PMID: 1650809

31. DiFranco M, Yu C, Quinonez M, Vergara JL. Inward rectifier potassium currents in mammalian skeletal muscle fibres. J Physiol. 2015; 593(5):1213–38. https://doi.org/10.1113/jphysiol.2014.283648 PMID: 25545278; PubMed Central PMCID: PMCPMC4358681.

32. Gallant JR, Traeger LL, Volkening JD, Moffett H, Chen P- H, Novina CD, et al. Genomic basis for the convergent evolution of electric organs. Science. 2014; 344(6191):1522–5. https://doi.org/10.1126/science.1254432 PMID: 24970089

33. Gotter AL, Kaetzel MA, Dedman JR. Electrophorus electricus as a model system for the study of membrane excitability. Comp Biochem Physiol A Mol Integr Physiol. 1998; 119(1):225–41. PMID: 11253789.

34. Bennett MVL. Electric Organs. In: Hoar WS, Randall DJ, editors. Fish Physiology. 5. New York: Academic Press; 1971. p. 347–491.

35. Abbott GW, Butler MH, Bendahhou S, Dalakas MC, Ptacek LJ, Goldstein SA. MiRP2 forms potassium channels in skeletal muscle with Kv3.4 and is associated with periodic paralysis. Cell. 2001; 104(2):217–31. Epub 2001/02/24. PMID: 11207363.

36. Izhikevich EM. Dynamical systems in neuroscience: the geometry of excitability and bursting. Cambridge, Mass.: MIT Press; 2007. xvi, 441 p. p.

37. Bastian J. Electrolocation in the presence of jamming signals: electroreceptor physiology. Journal of Comparative Physiology A: Neuroethology, Sensory, Neural, and Behavioral Physiology. 1987; 161(6):825–36. Epub 1987/11/01. PMID: 3430414.

38. Bastian J. Electrolocation in the presence of jamming signals: behavior. Journal of Comparative Physiology A: Neuroethology, Sensory, Neural, and Behavioral Physiology. 1987; 161(6):811–24. Epub 1987/11/01. PMID: 3430413.

39. Heiligenberg W. Electrolocation of objects in the electric fish *Eigenmannia* (Rhamphichthyidae, Gymnotoidei). Journal of Comparative Physiology. 1973; 87(2):137–64. https://doi.org/10.1007/Bf01352158 PubMed PMID: WOS:A1973R189500002.

40. Shifman AR, Lewis JE. The complexity of high-frequency electric fields degrades electrosensory inputs: implications for the jamming avoidance response in weakly electric fish. J R Soc Interface. 2018; 15(138). Epub 2018/01/26. https://doi.org/10.1098/rsif.2017.0633 PMID: 29367237.

41. Zhang TY, Ji S, Bozovic D. Synchronization of Spontaneous Active Motility of Hair Cell Bundles. PLoS One. 2015; 10(11):e0141764. https://doi.org/10.1371/journal.pone.0141764 PMID: 26540409; PubMed Central PMCID: PMCPMC4634766.

42. Salazar VL, Krahe R, Lewis JE. The energetics of electric organ discharge generation in gymnotiform weakly electric fish. J Exp Biol. 2013; 216(Pt 13):2459–68. https://doi.org/10.1242/jeb.082735 PMID: 23761471.

43. Kirschbaum F, Schwassmann HO. Ontogeny and evolution of electric organs in gymnotiform fish. Journal of Physiology, Paris. 2008; 102(4–6):347–56. Epub 2008/11/06. doi: S0928-4257(08)00048-X [pii] https://doi.org/10.1016/j.jphysparis.2008.10.008 PMID: 18984049.

44. Schwassmann HO, Assuncao MI, Kirschbaum F. Ontogeny of the electric organs in the electric eel, Electrophorus electricus: physiological, histological, and fine structural investigations. Brain Behav Evol. 2014; 84(4):288–302. https://doi.org/10.1159/000367884 PMID: 25428716.

45. Reardon EE, Parisi A, Krahe R, Chapman LJ. Energetic constraints on electric signalling in wave-type weakly electric fishes. J Exp Biol. 2011; 214(Pt 24):4141–50. Epub 2011/11/26. https://doi.org/10.1242/jeb.059444 PMID: 22116756.

46. Ferrari MB, McAnelly ML, Zakon HH. Individual variation in and androgen-modulation of the sodium current in electric organ. J Neurosci. 1995; 15(5 Pt 2):4023–32. Epub 1995/05/01. PMID: 7751963.

47. McAnelly ML, Zakon HH. Coregulation of voltage-dependent kinetics of Na^+ and K^+ currents in electric organ. J Neurosci. 2000; 20(9):3408–14. PMID: 10777803.

48. Graydon CW, Cho S, Diamond JS, Kachar B, von Gersdorff H, Grimes WN. Specialized postsynaptic morphology enhances neurotransmitter dilution and high-frequency signaling at an auditory synapse. J Neurosci. 2014; 34(24):8358–72. https://doi.org/10.1523/JNEUROSCI.4493-13.2014 PMID: 24920639; PubMed Central PMCID: PMC4051984.

49. Fonseca-Azevedo K, Herculano-Houzel S. Metabolic constraint imposes tradeoff between body size and number of brain neurons in human evolution. Proc Natl Acad Sci U S A. 2012; 109(45):18571–6. Epub 2012/10/24. https://doi.org/10.1073/pnas.1206390109 PMID: 23090991; PubMed Central PMCID: PMCPmc3494886.

50. Moroz LL, Kocot KM, Citarella MR, Dosung S, Norekian TP, Povolotskaya IS, et al. The ctenophore genome and the evolutionary origins of neural systems. Nature. 2014; 510(7503):109–14. https://doi.org/10.1038/nature13400 PMID: 24847885

51. MacIver MA, Patankar NA, Shirgaonkar AA. Energy-information trade-offs between movement and sensing. PLoS Comp Biol. 2010; 6(5):e1000769. Epub 2010/05/14. https://doi.org/10.1371/journal.pcbi.1000769 PMID: 20463870; PubMed Central PMCID: PMC2865506.

52. Markham MR, Ban Y, McCauley AG, Maltby R. Energetics of Sensing and Communication in Electric Fish: A Blessing and a Curse in the Anthropocene? Integr Comp Biol. 2016; 56(5):889–900. https://doi.org/10.1093/icb/icw104 PMID: 27549201